AGU PUBLICATIONS

JGR

Journal of Geophysical Research: Planets

RESEARCH ARTICLE
10.1002/2016JE005112

This article is a companion to *Horgan et al.* [2017] doi:10.1002/2016JE005111.

Key Points:
- Alteration morphology is strongly controlled by the pH of the alteration solution and the crystallinity of the starting material
- Acid alteration at low pH produces significant silica enrichment that is detectable in the near- and thermal infrared spectra
- Glassy materials develop thick silica-rich alteration layers that are spectrally consistent with large regions of the Martian surface

Supporting Information:
- Supporting Information S1

Correspondence to:
R. J. Smith,
rebeccajsmith@purdue.edu

Citation:
Smith, R. J., B. H. N. Horgan, P. Mann, E. A. Cloutis, and P. R. Christensen (2017), Acid weathering of basalt and basaltic glass: 2. Effects of microscopic alteration textures on spectral properties, *J. Geophys. Res. Planets*, *122*, 203–227, doi:10.1002/2016JE005112.

Received 17 JUN 2016
Accepted 29 DEC 2016
Accepted article online 3 JAN 2017
Published online 24 JAN 2017

Acid weathering of basalt and basaltic glass: 2. Effects of microscopic alteration textures on spectral properties

Rebecca J. Smith[1,2], Briony H. N. Horgan[2], Paul Mann[3], Edward A. Cloutis[3], and Philip R. Christensen[1]

[1]School of Earth and Space Exploration, Arizona State University, Tempe, Arizona, USA, [2]Department of Earth, Atmospheric, and Planetary Sciences, Purdue University, West Lafayette, Indiana, USA, [3]Department of Geography, University of Manitoba, Winnipeg, Manitoba, Canada

Abstract Acid alteration has long been proposed for the Martian surface, and so it is important to understand how the resulting alteration textures affect surface spectra. Two basaltic materials of varying crystallinity were altered in two different H_2SO_4 solutions (pH 1 and pH 3) for 220 days. The unaltered and altered samples were studied in the visible and near infrared (VNIR) and thermal infrared (TIR), and select samples were chosen for scanning electron microscopy analysis. Materials altered in pH 3 solutions showed little to no physical alteration, and their spectral signatures changed very little. In contrast, all materials altered in pH 1 acid displayed silica-rich alteration textures, and the morphology differed based on starting material crystallinity. The more crystalline material displayed extensive alteration reaching into the sample interiors and had weaker silica spectral features. The glass sample developed alteration layers tens of microns thick, exhibiting amorphous silica-rich spectral features that completely obscured the substrate. Thus, the strong absorption coefficient of silica effectively decreases the penetration depth of TIR spectral measurements, causing silica abundances to be grossly overestimated in remote sensing data. Additionally, glass samples with silica layers exhibited distinct concave up blue spectral slopes in the VNIR. Spectra from the northern lowland plains of Mars are modeled with high abundances of amorphous silica and exhibit concave up blue spectral slopes and are thus consistent with acid altered basaltic glass. Therefore, we conclude that large regions of the Martian surface may have formed through the interaction of basaltic glass with strongly acidic fluids.

1. Introduction

Large expanses of the low-albedo regions in the northern lowland plains of Mars have been shown to be spectrally consistent with acid-leached basaltic glass after comparing visible to near-infrared (VNIR) spectral data from natural and laboratory samples to data from the Mars Express OMEGA (Observatoire pour la Minéralogie, l'Eau, les Glaces, et l'Activité) imaging spectrometer [*Horgan and Bell*, 2012]. These same regions on Mars have thermal infrared (TIR) spectra that are modeled as requiring high abundances of amorphous high-silica material [*Bandfield*, 2002; *Rogers and Christensen*, 2007]. Subsequent studies found that Hawaiian basaltic glasses naturally altered in acidic fluids have TIR spectra dominated by an amorphous silica signature [*Minitti et al.,* 2007]. In the companion paper to this study, natural basalt, basaltic glass, and glass-bearing basalt exposed to strong acid in a laboratory setting were also found to have TIR spectra indicating significant concentrations of amorphous silica [*Horgan et al.,* 2017]. Comparison to laboratory TIR spectra thus supports the hypothesis that acid-leached basaltic materials may be present in the northern lowlands of Mars. Furthermore, very similar but more moderate high-silica TIR spectral signatures are commonly observed in dark terrains across the planet [*Bandfield et al.,* 2000; *Bandfield*, 2002; *Rogers and Christensen*, 2007], suggesting that acid-altered basaltic materials may in fact be present across large regions of the Martian surface.

Spectral analyses of laboratory acid-leached basalt and basaltic glasses suggest that the degree of alteration is largely determined by the pH of the alteration fluid and the crystallinity of the sample [*Horgan et al.,* 2017]. Basaltic materials altered under very low pH fluids (starting pH ~1) display strong spectral signatures associated with amorphous silica-rich phases, while the same materials altered under slightly higher pH fluids (starting pH ~3) show very little spectral change [*Horgan et al.,* 2017]. Additionally, acid-leached crystalline basalt and glass-rich basaltic materials are spectrally distinct from acid-leached basaltic glass at

both visible and near-infrared (VNIR and TIR wavelengths, even when altered under similar conditions (pH and duration of experiment)). For example, glassy basalt samples altered under very low pH fluids (starting pH ~1) display both mafic and amorphous silica-rich phase spectral signatures, whereas basaltic glass altered under the same conditions only display amorphous silica-rich phase spectral signatures. These spectral variations indicate physical and compositional differences between the alteration materials that form on the different glassy versus crystalline substrates and suggest different pathways to alteration. Understanding what factors affect the spectral variations in altered basaltic materials is important for the interpretation of remote sensing data and can help constrain the composition and weathering history of large regions of the Martian surface.

This study attempts to (1) describe and categorize the effects of acid alteration on basaltic materials of varying chemistry and glass content, (2) determine how physical and compositional differences between altered basaltic materials affect the VNIR and TIR spectral signatures, as reported in our companion paper [*Horgan et al.,* 2017], and (3) speculate how the alteration pathways differ with solution pH and parent material crystallinity. We use scanning electron microscopy (SEM) and Energy Dispersive X-ray Spectroscopy (EDS) to investigate the microscopic and compositional properties of the parent materials as well as the properties of the samples after exposure to sulfuric acid solutions of starting pH 1 and 3. Here we focus on amorphous silica coating and rind formation because it is so pervasive in natural systems; it is easily measured in the infrared spectra of altered basaltic substances, and the spectral effects of this type of surface alteration are poorly understood.

2. Background

2.1. Silicate Dissolution Mechanisms

A great number of laboratory studies have tried to understand and describe multioxide silicate mineral dissolution mechanisms, the results of which indicate that silicate minerals can dissolve either stoichiometrically (congruently) or nonstoichiometrically (incongruently) [*Oelkers*, 2001, and references therein]. Incongruent, or nonstoichiometric dissolution, is assumed to be taking place when the elemental molar ratios measured in a fluid are different from those in the solid [*Schott et al.,* 1981]. Studies in which silicate dissolution appears to be incongruent also report silica-rich layers depleted in low-valence cations found on the surfaces of the silicate substrates. Two competing dissolution mechanisms are commonly invoked to explain apparent incongruent dissolution and the accompanying silica-rich surface layers: (1)leaching, which involves the solid state interdiffusion of network-modifying cations followed by the hydrolysis of Si-O bonds [e.g., *Luce et al.,* 1972; *Paces*, 1973; *Oelkers*, 2001; *Schott et al.,* 2012], and (2) dissolution-reprecipitation, which involves the congruent dissolution of the multioxide mineral coupled with the reprecipitation of a secondary phase (most often an amorphous silica-rich phase) [e.g., *O'Neil and Taylor*, 1967; *Hellmann et al.,* 2003, 2004; *Daval et al.,* 2011; *King et al.,* 2011].

For decades, leaching has been the favored explanation for the apparent incongruent dissolution of many silicate minerals. During the leaching process in acidic conditions, weaker monovalent metal-oxide bonds break more rapidly than divalent or trivalent metal-oxide bonds, which break faster than Si-O bonds [*Schott et al.,* 2009]. The Si-O structure is finally broken when Al cations are exchanged for protons, leaving behind partially detached Si atoms that are more readily removed from the structure [*Oelkers*, 2001; *Schott et al.,* 2009]. Thus, the leaching mechanism is consistent with nonstoichiometric elemental release rates and can also explain the amorphous silica-enriched layers that commonly form on the silicate mineral surfaces after dissolution.

Currently, there is growing evidence that multioxide silicate mineral dissolution is more consistent with a dissolution-reprecipitation mechanism than a leaching mechanism, as will be discussed in section 2.3 [e.g., *O'Neil and Taylor*, 1967; *Hellmann et al.,* 2003, 2004, 2012; *Ruiz-Agudo et al.,* 2012, 2014; *Putnis and Ruiz-Agudo*, 2013; *Gin et al.,* 2013]. In fact, *Hellmann et al.* [2012] argue that dissolution-reprecipitation is the unifying, fundamental mechanism behind all mineral dissolution, whether the calculated cation release rate is stoichiometric or not. In this model, the dissolution reactions take place in a supersaturated boundary layer of fluid between the parent and reprecipitated product surfaces [*Hellmann et al.,* 2012; *Ruiz-Agudo et al.,* 2012]. Additionally, in this model all crystalline phases undergo stoichiometric dissolution within the boundary layer, but the reprecipitation of silica-rich phases removes cations from the bulk

solution, which can make the elemental molar ratios between solid and fluid appear incongruent. Thus, the dissolution-reprecipitation mechanism can explain the amorphous silica-enriched layers commonly associated with apparent incongruent dissolution and also addresses the problem that "leaching" was noted to occur in basic pH systems where proton-cation exchange would not be relevant [*Hellmann et al.,* 2012].

Similarly, the dissolution mechanisms for amorphous silicate glasses have also long been debated. Silicate glasses, like minerals, frequently form silica-rich surface layers as a result of dissolution experiments and the layers are commonly ascribed to leaching processes [e.g., *Doremus*, 1975; *Guy and Schott*, 1989; *Petit et al.,* 1990; *Oelkers and Gislason*, 2001]. Yet *Crovisier et al.* [1987] were among the first to suggest that the structure and chemistry of silica-rich layers on basaltic glass indicates that they form through precipitation from solution after congruent dissolution of the silicate. More recent studies support this observation [*Geisler et al.,* 2010, 2015; *Gin et al.,* 2013], as will be discussed in section 2.3.

2.2. Terminology of Silica-Enriched Surface Altered Layers

As noted above, amorphous silica is a common product that accompanies mineral and glass dissolution. The literature describes many different forms of amorphous silica enrichment in naturally and synthetically weathered samples, each form implying a formation mechanism. In order to avoid confusing terminology in this study, we classify the potential forms of silica enrichment into three different texture categories based primarily on silica source and formation mechanism. These categories are (1) coatings, (2) leached rinds, also sometimes called leached layers, and (3) precipitated layers or zones. When we want to describe silica enrichment without evoking a specific mechanism or silica source, we will refer to such features as "silica-enriched surface altered layers (or zones)."

Silica coatings are accreted layers on a rock or grain surface that have been formed via precipitation out of a bulk solution. The main distinguishing property of silica coatings is that the silica is derived from an external source, it comes whether from dissolved silicate dust particles or from a source that is millimeters to meters away [*Dorn*, 1998]. The key point is that the silica is transported to the surface and is not derived from the substrate itself [*Dixon et al.,* 2002].

Unlike rock coatings, both leached rinds and precipitated layers are surface altered layers thought to form through the dissolution of the substrate. As there is much debate surrounding the dissolution mechanisms of silicate minerals and glasses, there is also confusion about the terminology of the dissolution alteration products. Leached layers indicate surface altered layers resulting from the leaching (incongruent dissolution) mechanism [e.g., *Casey et al.,* 1989a, 1989b, 1993; *Petit et al.,* 1989, 1990], whereas precipitated layers form via the dissolution-reprecipitation mechanism [e.g., *Crovisier et al.,* 1987; *Hellmann et al.,* 2003, 2004, 2012; *Ruiz-Agudo et al.,* 2014].

2.3. Previous Microscopic Studies of Alteration Texture Morphology

Alteration texture morphology and chemistry can help distinguish between the different silica-enriched surface altered layers described above. A number of previous studies have used various forms of microscopy and supporting elemental measurements to describe and characterize silica-enriched alteration textures. Here we use their results to determine distinguishing morphological and chemical properties, allowing us to identify the potential formation mechanisms for the alteration textures observed in this study.

Silica coatings are generally characterized by having sharp compositional and morphological boundaries between the coating and the substrate [*Farr and Adams*, 1984; *Dorn*, 1998]. Compositionally, silica coatings are mostly made of X-ray amorphous silica but can contain varying abundances of iron and aluminum [*Dorn*, 1998]. Additionally, silica coatings frequently incorporate other material such as dust and/or crystalline particles [*Dorn*, 1998]. Thicknesses derived from SEM images range from microns to almost a millimeter [*Dorn*, 1998]. The coatings generally appear as accreted layers in cross section [*Farr and Adams*, 1984; *Dorn*, 1998] and cannot form over void spaces [*Chemtob et al.,* 2010].

Aside from apparent incongruent cation release rates, the strongest argument for a leached rind has been the presence of a sigmoidal elemental profile between the rind and the substrate [e.g., *Nesbitt and Muir*, 1988; *Casey et al.,* 1989b; *Petit et al.,* 1989, 1990; *Shotyk and Nesbitt*, 1992], which has been used to argue for a diffusive reaction surface. However, mathematical modeling and direct measurements have shown

that an ion or electron probe diameter is effectively broadened by the scattering of radiation from some depth [e.g., *Ganguly et al.,* 1988; *Belkorissat et al.,* 2004], which creates a spatial averaging effect that produces a diffuse elemental profile (hundreds of nanometers thick) [*Hellmann et al.,* 2003, 2004]. Thus, commonly used elemental measurement techniques such as secondary ion mass spectroscopy and EDS systems (found on SEM instruments) tend to produce diffuse elemental profiles. Advances in transmission electron microscopy (TEM) indicate that the chemical boundary between the layers and the substrate might actually be much sharper (<4–7 nm) [e.g., *Hellmann et al.,* 2004; *Gin et al.,* 2013]. *Hellmann et al.* [2003, 2004] considered the sharp chemical boundary to be evidence for dissolution-reprecipitation mechanisms, calling into question the legitimacy of previously designated "leached" layers. While there is uncertainty about the formation mechanism for previously studied surface altered layers, we will honor the original researcher's designation as leached or "precipitated" layer in the following discussion of alteration texture morphology and chemistry.

Leached rinds are residual material left behind after incomplete dissolution of the parent material. It is thought that the silica in the leached rind undergoes restructuring during rind formation [*Casey et al.,* 1993; *Tsomaia et al.,* 2003] including repolymerization [e.g.,*Casey et al.,* 1993; *Schweda et al.,* 1997], recrystallization [*Banfield et al.,* 1995], and structural collapse [*Paces*, 1973]. Surface altered layers that are designated as leached rinds are generally quite thin with thicknesses ranging from 50 nm to 10 μm [e.g., *Casey et al.,* 1993; *Minitti et al.,* 2007]. According to *Minitti et al.* [2007], experimentally produced leached layers are rarely pure SiO_2. For example, *Berger et al*. [1987] reported a leached layer with ~15 wt % Al_2O_3. Additionally, leached layers are commonly described as being fractured and brittle and may detach from the underlying surface [*Gislason and Oelkers*, 2003; *Tosca et al.,* 2005; *Schott et al.,* 2009, 2012; *Chemtob et al.,* 2010; *Seelos et al.,* 2010].

Silica-enriched precipitated layers and zones (silica-enriched regions occurring within a substrate) are formed when the parent material is first completely dissolved, releasing the oxides that are reprecipitated onto the surface of the parent material. Surface altered layers that are designated as precipitated layers vary in thickness between ~5 to 870 nm on various silicate minerals [*Hellmann et al.,* 2012] and 10–300 μm on borosilicate glasses [*Geisler et al.,* 2010]. Precipitated layers and zones are indicated by very abrupt (nanometer scale) chemical and morphologic boundaries between the layer and the substrate [*Hellmann et al.,* 2004, 2012], though, as discussed above, the chemical profile depends strongly on the measurement technique. Precipitated layers and zones are made of mostly hydrous SiO_2 but frequently contain traces of other ions such as Al^{3+}, Ca^{2+}, and Mg^{2+} [*Hellmann et al.,* 2012]. Precipitated layers and zones essentially replace the parent material with a more stable amorphous phase, and replacement reactions commonly involve volume changes, both positive (expansion) and negative (shrinkage), which can generate stresses sufficient to cause fracturing in and between the parent and product phases [*Ruiz-Agudo et al.,* 2014].

Minitti et al. [2007] and *Chemtob et al.* [2010] have used microscopic analyses to distinguish between silica coatings, leached rinds, and precipitated layers on naturally weathered basaltic samples from Hawaiian lava flows. *Minitti et al.* [2007] investigated a number of coated samples collected from various vents and flows in both desert and more humid climates within the Hawaii Volcanoes National Park. They described three main silica layer morphologies: marbled, nonporous, and mineral bearing. They concluded that the marbled and nonporous morphologies were consistent with either leaching or dissolution-reprecipitation mechanisms but that, based on observed thicknesses (~2–80 μm thick), the morphologies were most similar to precipitated layers. They also concluded that the mineral-bearing morphology must have resulted from the cementation of airfall deposited tephra. *Chemtob et al.* [2010] studied a suite of coated samples from the Kilauea December 1974 flow collected in a number of locations in the Ka'u Desert. They described continuous silica-rich layers (~10 μm thick) with veined textures of crisscrossing fractures and observed at least one location where the layer overlaid a near-surface vesicle. They also detected jarosite, a sulfate mineral that forms in strongly acidic environments, within the silica layers. The silica layers ended at the substrate with sharp chemical boundaries, though *Chemtob et al.* [2010] noted that a leached layer could be thinner than the spatial resolution of the measurement technique. Based on their observation of the layer over the vesicle, they concluded that the silica layers must have formed in situ rather than via a depositional coating formation mechanism. The authors favored the leaching mechanism as the main formation mechanism based on the detection of jarosite, which argued for favorable leaching conditions. However, the authors also noted that micrometer-scale dissolution-reprecipitation could have taken place.

2.4. Spectral Identification and Effects of Silica-Enriched Alteration Textures

Silica-enriched surface altered layers are found in nearly all environments on Earth and are potentially significant components of the Martian surface. Most of our knowledge of the composition of the Martian surface comes from spectroscopic observations, and so it is important to understand how silica-enriched surface layers affect planetary surface spectra. A number of studies have attempted to define the spectral characteristics of natural [e.g., *Kahle et al.,* 1988; *Crisp et al.,* 1990; *Christensen and Harrison Thliveris*, 1993; *Michalski et al.*, 2004; *Michalski et al.,* 2006; *Minitti et al.,* 2007; *Seelos et al.,* 2010] and synthetic [*Kraft et al.,* 2003] samples. Here we summarize some of the findings and see that the effects are complicated and are still poorly understood.

The information received from spectral measurements is highly dependent on the range of the wavelengths being measured. For instance, penetration depth, which is important to this study, generally increases with increasing wavelength; visible and near-infrared (VNIR; 0.35 to 2.5 μm) wavelengths measure only the outer few microns of a sample, whereas the thermal infrared (TIR; 5 to 50 μm) wavelengths are able to penetrate a depth of up to ~100 μm. Additionally, VNIR reflectance and TIR emission spectroscopy divulge different information about the mineralogy (composition and structure) of the sample. Visible wavelength measurements are highly sensitive to electron transitions, while infrared measurements are sensitive to molecular vibrations. Water and hydroxyl (OH) molecules have strong vibrational overtones at 1.4 and 1.9 μm and are easily detected using near-infrared spectroscopy [e.g., *Clark et al.,* 1990]. Most rock forming functional groups [*Clark et al.,* 1979] (SiO_4, SO_4, and CO_3) have fundamental vibrations between ~7 and 12.0 μm, so that they are easily detected in thermal infrared spectroscopy. Thus, VNIR spectroscopy is important for detecting Fe-bearing and hydrated minerals, while TIR spectroscopy is especially important for detecting silicates. The combination of both measurements provides a more complete view of the sample than either could offer on their own.

Pure hydrated amorphous silica (opal-A) has an identifiable spectrum in the TIR with a Si-O stretching feature at ~1115 cm^{-1} (where x cm^{-1} = 10,000/y μm), a corresponding shoulder at 1220 cm^{-1}, and a Si-O bending feature at ~465 cm^{-1}. Likewise, in the VNIR, opal-A has hydration features located at 1.4 μm and 1.9 μm and a broad doublet spectral band near 2.21 and 2.26 μm due to SiOH rotation and stretching vibrational modes [*Langer and Flörke*, 1974; *Rice et al.,* 2013]. However, most natural silica coatings and surface altered layers are not pure silica [e.g., *Dorn*, 1998; *Farr and Adams*, 1984; *Minitti et al.,* 2007; *Chemtob et al.,* 2010], and the inclusion of Al^{3+}, Fe^{3+}, Mg^{2+}, and Ca^{2+} in the structure causes a decrease in the degree of polymerization of the framework structure. In the TIR, the position of the Si-O stretching feature is positively correlated to the degree of polymerization of the silica tetrahedral network [*White and Minser*, 1984; *Crisp et al.,* 1990; *Michalski et al.,* 2005]. Thus, the TIR Si-O stretching features of natural silica-rich alteration materials are generally shifted to slightly lower wave number (e.g., ~1100 cm^{-1}) [*Minitti et al.,* 2007].

Silica-rich coatings and surface altered layers can alter and obscure the visible and infrared spectrum of a substrate [*Kahle et al.,* 1988; *Crisp et al.,* 1990; *Abrams et al.,* 1991; *Kraft et al.,* 2003; *Minitti et al.,* 2007; *Seelos et al.,* 2010]. *Kraft et al.* [2003] created pure colloidal silica coatings of varying thickness on natural Columbia River basalt samples and found that silica coatings only ~6–10 μm thick can completely mask the TIR spectral signature of the underlying rock. They also found that coatings ~0.5 μm thick were sufficient to develop a weak silica spectral feature at ~1115 cm^{-1}. This feature grew in intensity with coating thickness until the spectral features of the substrate were obscured at ~6 μm. Coatings > ~3 μm thick also developed the 1220 cm^{-1} spectral shoulder feature associated with hydrated amorphous silica. Additionally, *Kraft et al.* [2003] found that when silica coatings were less than ~7 μm thick, the coating and substrate TIR spectra would not combine linearly to accurately model the measured sample spectrum, adding complication to the general assumption that surface spectra are linear mixtures of the components.

Similarly, amorphous silica-like spectral signatures tend to dominate the TIR spectra of natural silica-enriched surface altered layers on basalt and basaltic glass, sometimes completely obscuring the substrate [*Farr and Adams*, 1984; *Kahle et al.,* 1988; *Crisp et al.,* 1990; *Minitti et al.,* 2007; *Ruff et al.,* 2011]. *Crisp et al.* [1990] studied Hawaiian lava flows of different ages and found that a weak TIR spectral feature at ~1080–1086 cm^{-1} associated with silica-rich coatings developed in the spectra of flows that were only

Table 1. Sample Information

Sample Name	ICE170[a]	BAS101[a]
Sample description	Basalt, pillow lava (~50% glass)[b]	Basaltic Glass, subaerial flow (~75% glass)[b]
Sample location	Dagmalafell, Iceland	Kilauea Caldera, Hawaii, 1956 flow
Wt %[c]		
SiO_2	46.4	50.6
TiO_2	0.75	3.19
Al_2O_3	14.4	13.1
Fe_2O_3	11.0	1.07
FeO	8.39	10.6
MnO	0.17	0.18
MgO	13.0	6.38
CaO	13.4	10.7
Na_2O	1.35	3.05
K_2O	0.02	0.54
Total	100.5	99.4
Mineral abundances (%)[d]		
Plagioclase	37	No detectable crystalline phases[e]
Clinopyroxene	35	
Olivine	28	
Chromite	<3	
Total	~103	

[a]Collected by E. Cloutis.
[b]Glass abundances reported by *Horgan et al.* [2017] and derived using TIR spectral linear deconvolution methods.
[c]Major oxides for samples derived by X-ray fluorescence (XRF). Original data published in *Cloutis et al.* [2015].
[d]X-ray amorphous-free, mineral abundances derived by Rietveld analysis of X-ray diffraction (XRD) patterns. Original data published in *Cloutis et al.* [2015].
[e]No Rietveld analysis of the BAS101 XRD pattern was completed.

weeks old. This feature strengthened with increasing age at the expense of lower wave number (~925–950 cm^{-1}) and, thus, more mafic silicate features. Lava flows over 50 years old also develop the 1220 cm^{-1} shoulder feature associated with hydrated amorphous silica. Presumably, silica-rich coatings increase in thickness with age, affecting the combined coating and substrate spectra in manners similar to those observed by *Kraft et al.* [2003].

In the VNIR, leached rinds are generally distinguished from silica coatings by the lack of silica hydration bands at 2.21 and 2.26 μm and a concave up spectral slope [*Minitti et al.,* 2007; *Seelos et al.,* 2010; *Horgan and Bell*, 2012; *Horgan et al.,* 2017]. To date, the nonlinear concave up spectral shape has only been observed in glass-rich samples thought to have leached layers and is hypothesized to be due to wavelength-dependent scattering by structures at the submicron scale, perhaps related to surface textures in the rinds [*Horgan et al.,* 2017]. Coatings, on the other hand, exhibit a linear blue spectral slope (less reflectance at longer wavelengths) from the visible into the near infrared, regardless of their substrate [*Kraft et al.,* 2007; *Milliken et al.,* 2008].

3. Methods

3.1. Acid-Leaching Experiments

A subset of samples from *Horgan et al.* [2017] was selected for analysis, focusing on the samples that exhibited interesting spectral changes after the experiments. We observed the properties of unaltered and altered samples of two different starting materials that differ in both composition and degree of crystallinity [*Horgan et al.,* 2017] (see Table 1 for sample information): a partially glassy Icelandic olivine basalt from a subaqueous pillow lava (ICE170; ~50% glass) and a Hawaiian glassy basalt from a subaerial flow (BAS101; ~75% glass). Each basaltic hand sample was ground into sand-sized particles (500–1000 μm) using a mortar and pestle.

The acid-leaching experiment methods, summarized here, can be found in greater detail in our companion paper [*Horgan et al.,* 2017]. The experiments simulated an open hydrologic system. Samples were placed in acid solution baths, and fluids were frequently replaced with a fresh acid solution. Two stock acid solutions were made up using concentrated H_2SO_4 and distilled H_2O, with a pH of 1.0 and 3.0. Approximately 7 g

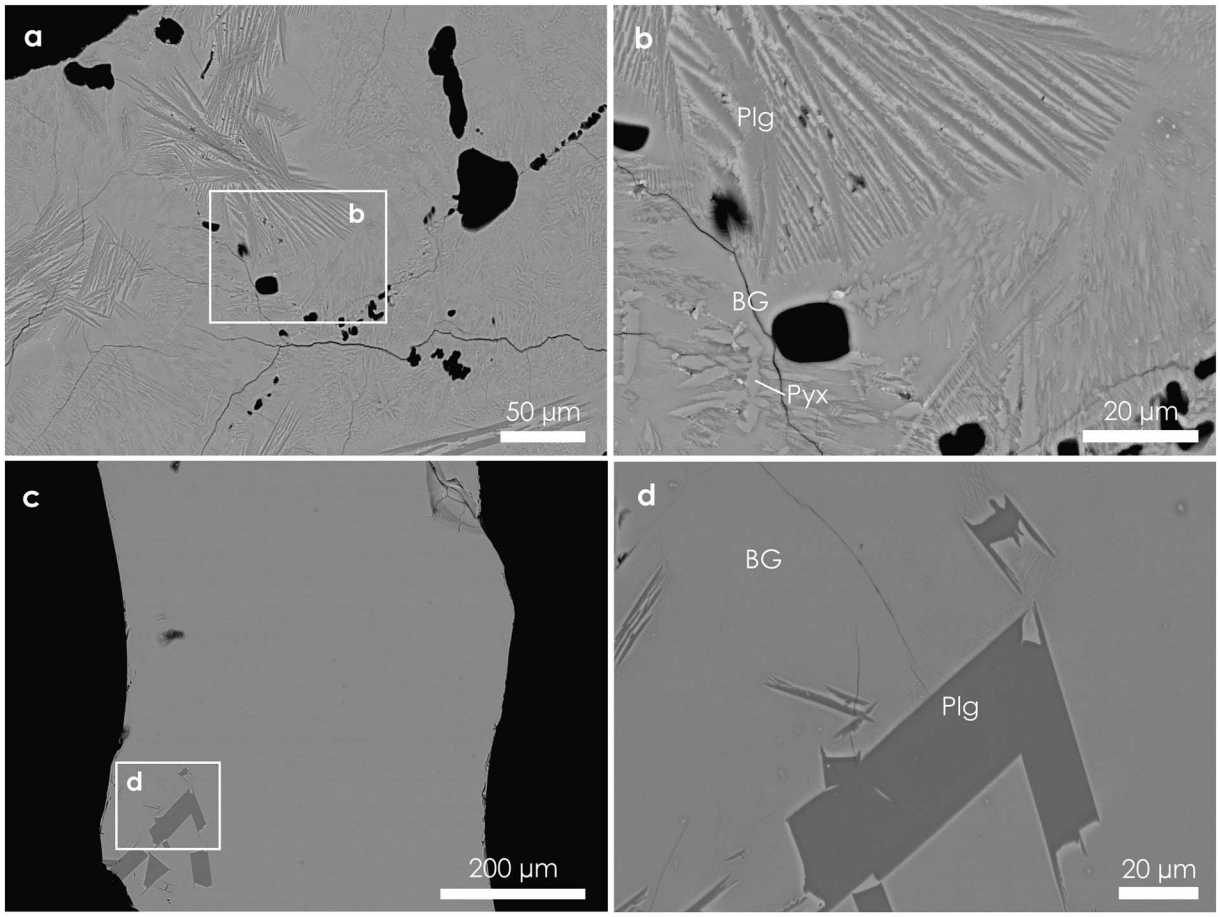

Figure 1. BSE images of starting material (a and b) ICE170 and (c and d) BAS101. White rectangles indicate regions enlarged in pictures on the right. Plg is plagioclase, Pyx is pyroxene, and BG is basalt glass.

of each sample was placed in separate Teflon vessels with 30 mL of the stock sulphuric acid solution and 10 mL of 30% H_2O_2. Hydrogen peroxide was chosen as the oxidizing agent because superoxides and peroxides have been suggested as candidates for the purported oxidant in Martian surface materials [*Zent and McKay*, 1994; *Golden et al.,* 2005]. In total, the samples were exposed to acid for 220 days at 25°C; however, alteration progress was periodically halted at different time steps in order to document how progressive alteration affected the spectra of the samples. All samples were washed with deionized water prior to analysis to remove loose secondary minerals, because our study was focused on analyzing physically adhered alteration rinds and coatings on the samples.

3.2. Scanning Electron Microscopy

In order to perform detailed microscopic analyses of the weathered particles, we randomly selected 3 grains of each starting material and 10 grains of each ending material from the experiments listed in Table 1 for scanning electron microscope (SEM) analysis. Grains were arranged on double-sided tape and then encapsulated in a two-part epoxy cured at room temperature. The sample stub was polished to 0.25 μm using progressively smaller-sized particle diamond suspension and diamond paste in order to get a cross-sectional view through the grains.

The sample stub was carbon coated and then examined at the Arizona State University Center for High-Resolution Electron Microscopy using an XL-30 SEM with a field emission source. Both secondary electron (SE) and backscattered electron (BSE) detectors were utilized to image the samples. SE images give information about sample topography and morphology, while BSE images inform about variations in composition across the sample since backscattering intensity is proportional to the mean atomic number. Semiquantitative chemistry was measured using spot and line analyses obtained from the Energy-

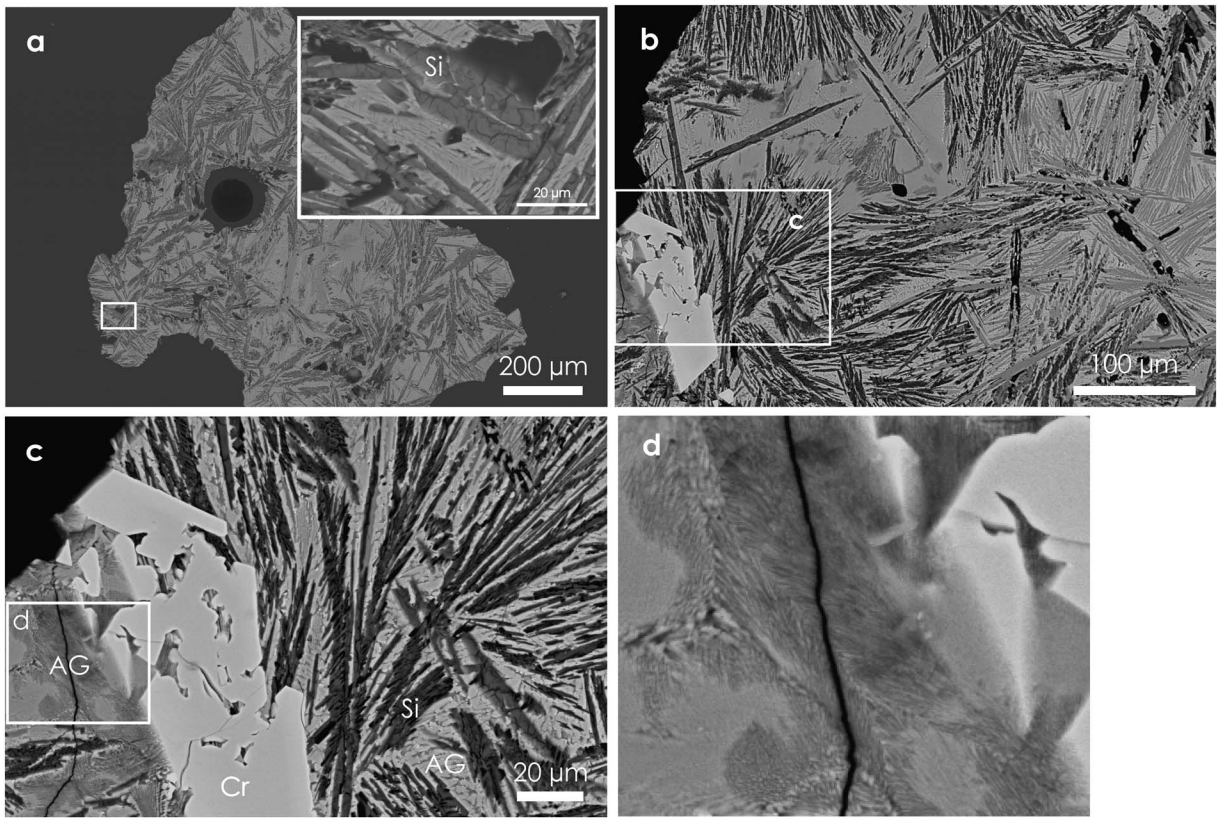

Figure 2. BSE images of ICE170 weathered in pH 1 acid for 220 days. (a) Overview of a grain showing heterogeneous interior alteration morphology and enlarged view (white box) showing the fractured nature of the Si-enriched zones (Si). (b) Context image of another grain with white box showing region enlarged in Figure 2c. (c) AG is altered glass, Cr is chromite, and Si is a silica-enriched phase. (d) Close-up of AG regions showing the feathered and mottled textures.

Dispersive X-ray Spectroscopy (EDS) system on the SEM. All SEM measurements were made at a working distance of 11 mm, an accelerating voltage of 20 kV, and a spot size of 3 or 4.

3.3. Spectroscopy

Here we summarize the methodology for spectral measurements, and the details can be found in *Horgan et al.* [2017]. Thermal infrared emission spectra (TIR) were measured at the Arizona State University Infrared Spectroscopy Laboratory using a Nicolet Nexus 670 spectrometer that is configured to measure emissivity [*Ruff et al.*, 1997]. Spectra were collected at a spectral resolution of 2 cm^{-1} over the range of 200–2000 cm^{-1}. The samples were heated to 80°C for multiple hours prior to being measured, and this temperature was maintained during spectral acquisition by actively heating the sample with a hotplate. All TIR spectral measurements were taken after the acid-leaching experiments were complete.

Visible and near-infrared (VNIR) reflectance spectra were collected from all the samples using an ASD FieldSpec Pro HR spectrometer over the wavelength range of 0.35 to 2.5 µm. A 150 W Quartz tungsten halogen light source was used to illuminate the samples, and reflectance spectra were measured at $i = 30°$, $e = 0°$; 200 spectra of each sample were collected periodically when the sample was removed from the acid bath and averaged to improve SNR. To reduce the effects of specular reflections, all 500–1000 µm samples were spun on a turntable at 33 rpm during data collection.

4. Results

4.1. SEM

In the following section, we use SEM observations to characterize the morphology and chemistry of the starting materials and their corresponding altered products. Doing so allows us to visualize any changes

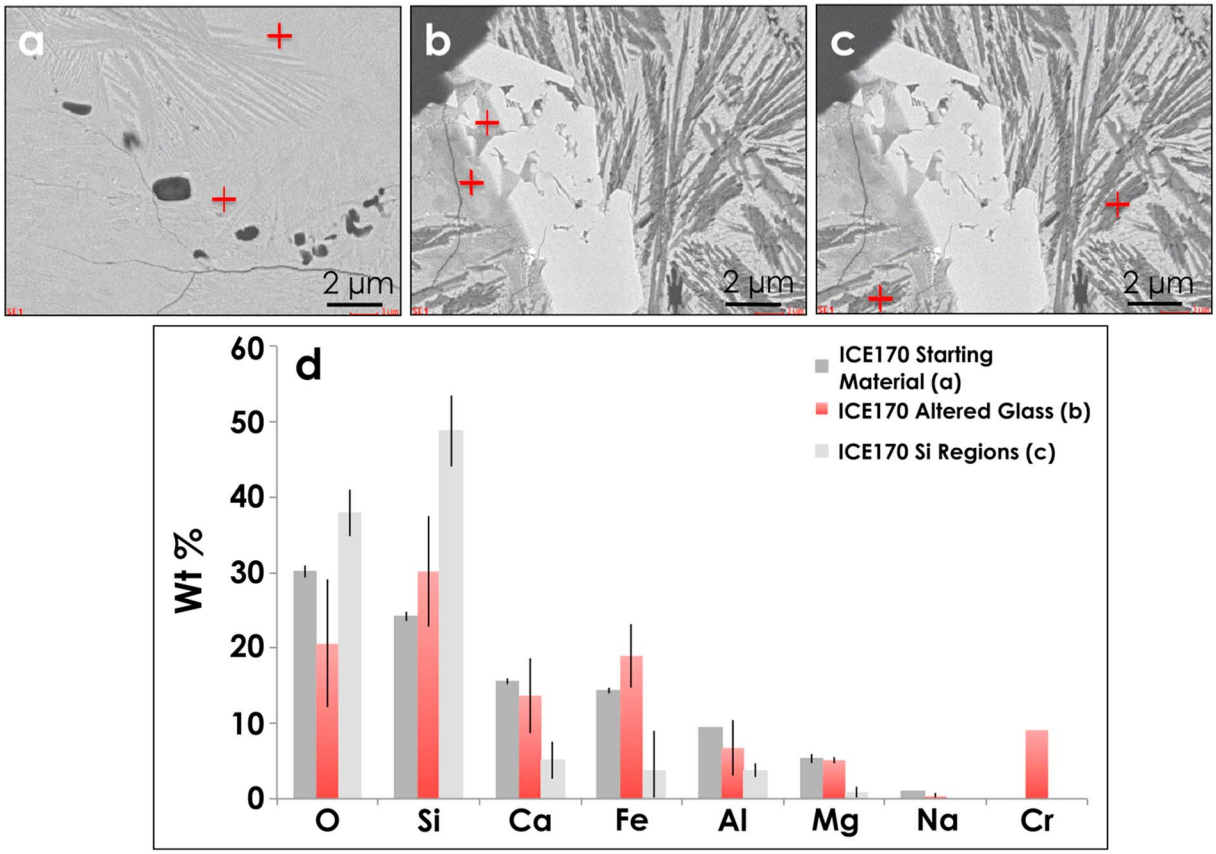

Figure 3. Locations of EDS point analyses (red crosses) for (a) basalt glass in ICE170 starting material, (b) altered glass in ICE170 exposed to starting pH ~1 acid solution for 220 days, and (c) Si-enriched regions in ICE170 exposed to starting pH ~1 acid solution for 220 days. (d) Average wt % of major elements from EDS point measurements for each phase type in Figures 3a–3c. Error bars represent one standard deviation.

made to the samples after exposure to acidic solutions. Also, comparing physical and chemical properties can highlight the differences between the materials that might affect their spectral properties.

4.1.1. Starting Material

The partially glassy sample (ICE170) is composed of plagioclase and pyroxene within the glassy matrix (Figures 1a and 1b). The plagioclase crystals are elongate and tend to form sheaf-like radial clusters, and pyroxene tends to form as crystallites. The crystal shapes indicate rapid quenching during formation. ICE170 grains exhibit numerous void spaces up to ~150 μm in diameter and fractures that reach up to

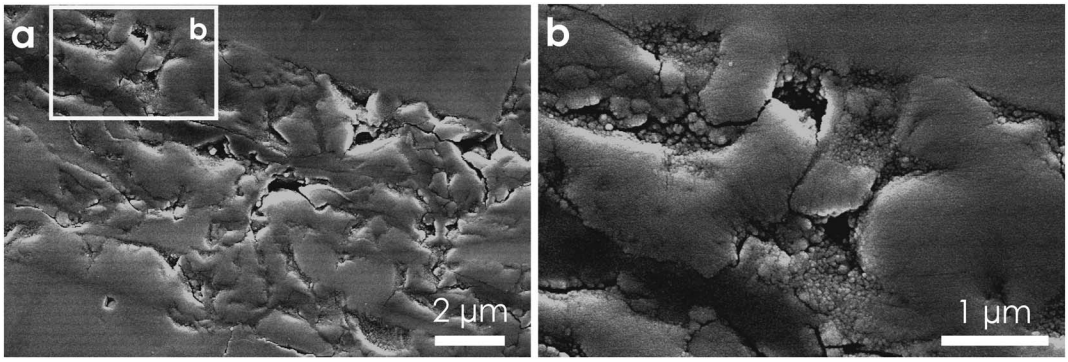

Figure 4. SE cross-sectional view of ICE170 grains mounted in epoxy after exposure to starting pH ~1 acid. (a) Shows the fractured topography of the altered regions within the grains, and upon closer inspection (b) spherical deposits/debris is visible within in the altered regions.

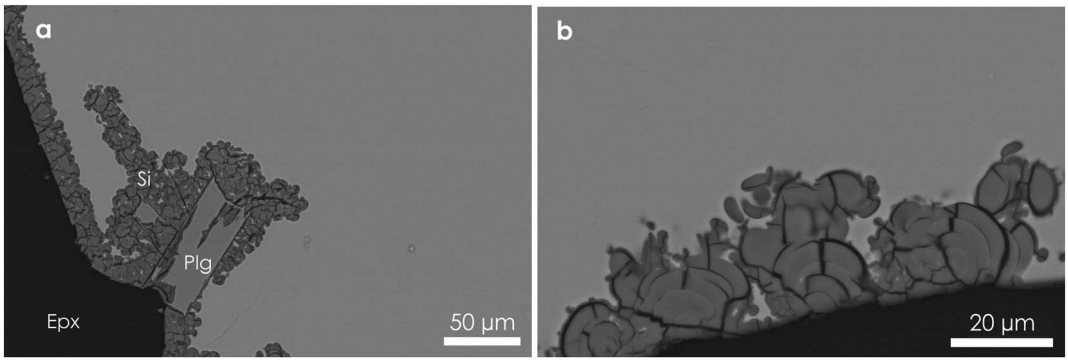

Figure 5. BSE images of BAS101 samples after exposure to starting pH ~1 acid solution. (a) Epx is epoxy, Plg is plagioclase, and Si is a silica-enriched alteration phase. The Si-enriched layer is nearly continuous around the perimeter of the grains and is a different phase than the grain interior. (b) Enlarged view showing the conchoidal fracturing associated with the silica-enriched alteration layer.

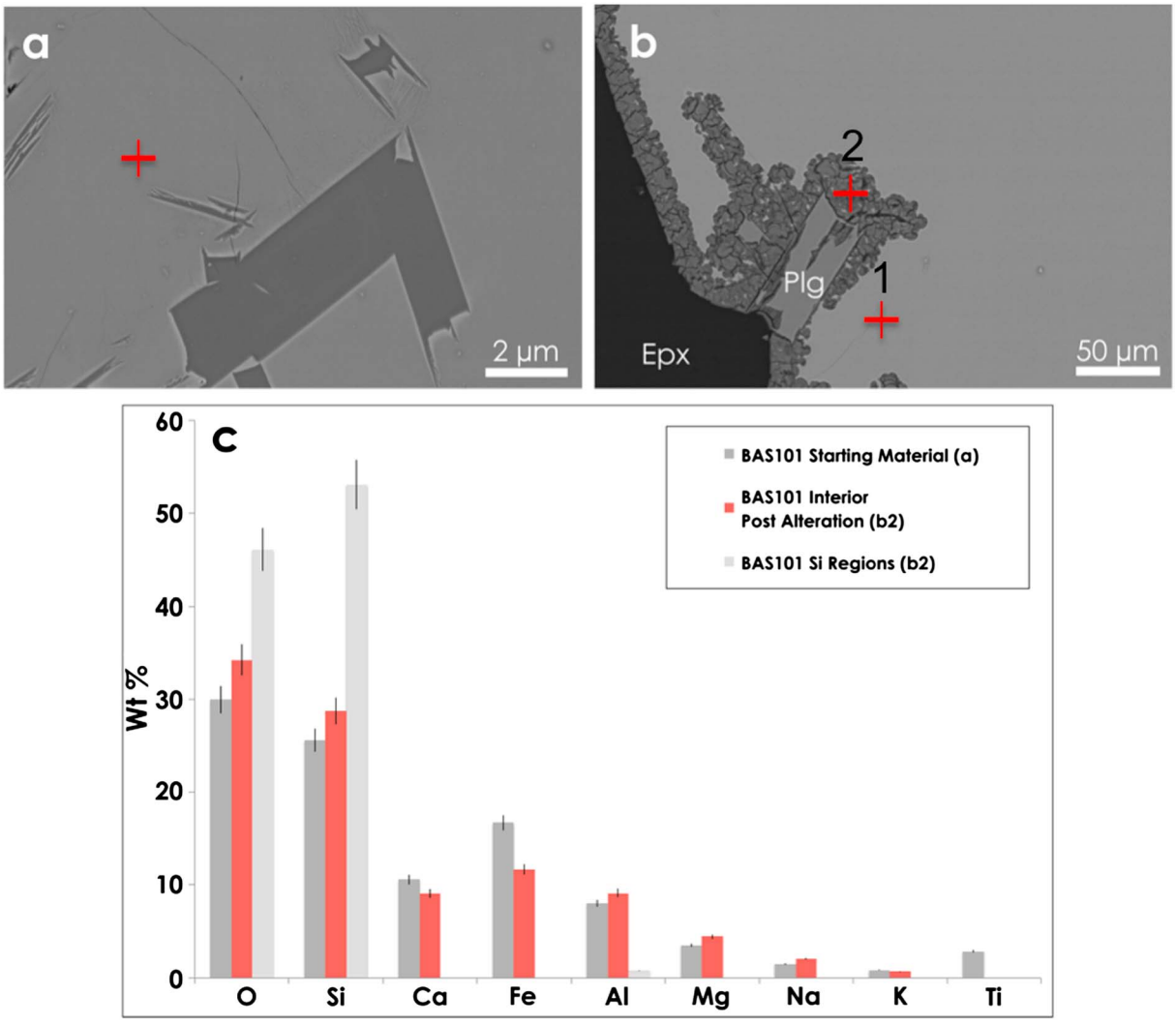

Figure 6. BSE images of BAS101 (a) starting material and (b) grain exposed to starting pH ~1 acid solution. Red crosses indicate the locations where EDS spot analyses were taken. (b) Spot analyses were taken from both the basaltic glass interior (1) and the Si-enriched layer (2). (c) Elemental wt % from EDS spot analyses.

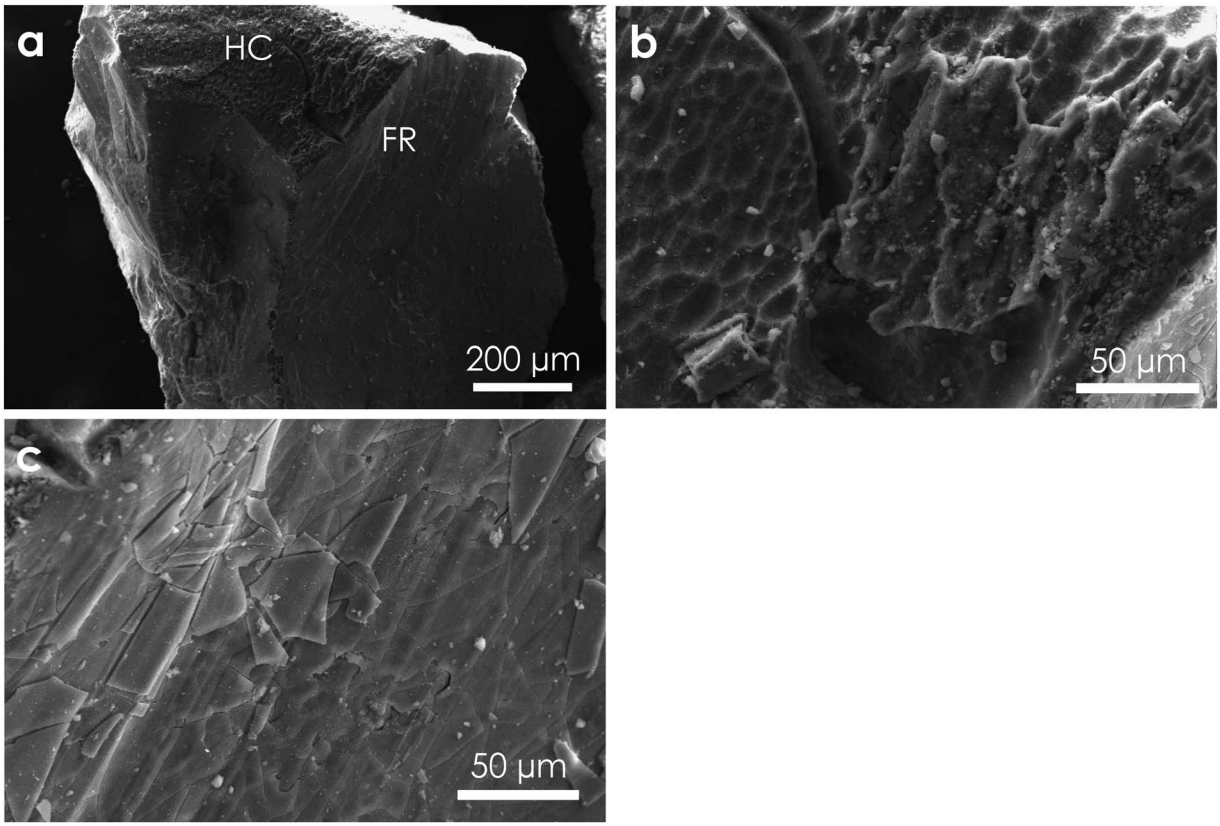

Figure 7. SE images BAS101 sample grain surfaces after exposure to starting pH ~1 acid solution. (a) Context image of an altered BAS101 grain showing relationship between HC (honeycomb texture) and FR (fractured texture). (b) Close-up of HC texture. (c) Close-up of FT.

~500 μm long, sometimes dissecting the grain. In contrast, the more glass-rich sample (BAS101) has only a few ~30–60 μm plagioclase crystals in each grain (Figures 1c and 1d). The fractures in BAS101 grains are relatively short (tens of microns in length) and are parallel or subparallel to the grain perimeters, not reaching into the grain interiors. Overall, the partially glassy basalt sample (ICE170) has more crystal boundaries, pores, and fractures than the basaltic glass sample (BAS101) (Figure 1). It should be noted that none of the starting material grains have evidence for secondary phases.

4.1.2. Glassy Basalt in Low pH Acid

BSE imaging reveals that glassy basalt (ICE170) grains exposed to starting pH ~1 acid solution do not have continuous surface altered layers. Rather, the relative contrast changes in the BSE images (Figure 2) and EDS point analyses (Figure 3) show that there are multiple alteration phases throughout the sample. We separate the altered areas into two different phases based on composition and morphology, "Si-enriched regions" and "altered glass." The Si-enriched regions are dark in BSE images, indicating fewer heavier elements (Figure 2c) than the surrounding phases, and have a fractured appearance (Figure 2a). In the BSE images, the altered glass areas are a shade of grey that is intermediate between the darker Si-enriched regions and the lighter basaltic glass and pyroxene crystallite-rich regions, indicating an intermediate composition (Figure 2c). The altered glass regions have a feathered texture at the submicron scale and a mottled texture at the micron scale, indicating that the altered glass composition is not homogeneous (Figure 2d).

Multiple EDS point analyses were averaged together to obtain an average composition for the starting basaltic glass material, the Si-enriched regions, and the altered glass (Figure 3; see Table S1 in the supporting information for wt % values). The Si-enriched regions exhibit a significant increase in Si and decrease in Na, Mg, Fe, and Ca from the starting material. Al abundance also decreases, but less dramatically. The average altered glass composition exhibits an increase in Si and Fe and a decrease in Na, Al, and Ca relative to the starting material. One of the points considered to be altered glass might include some altered chromite

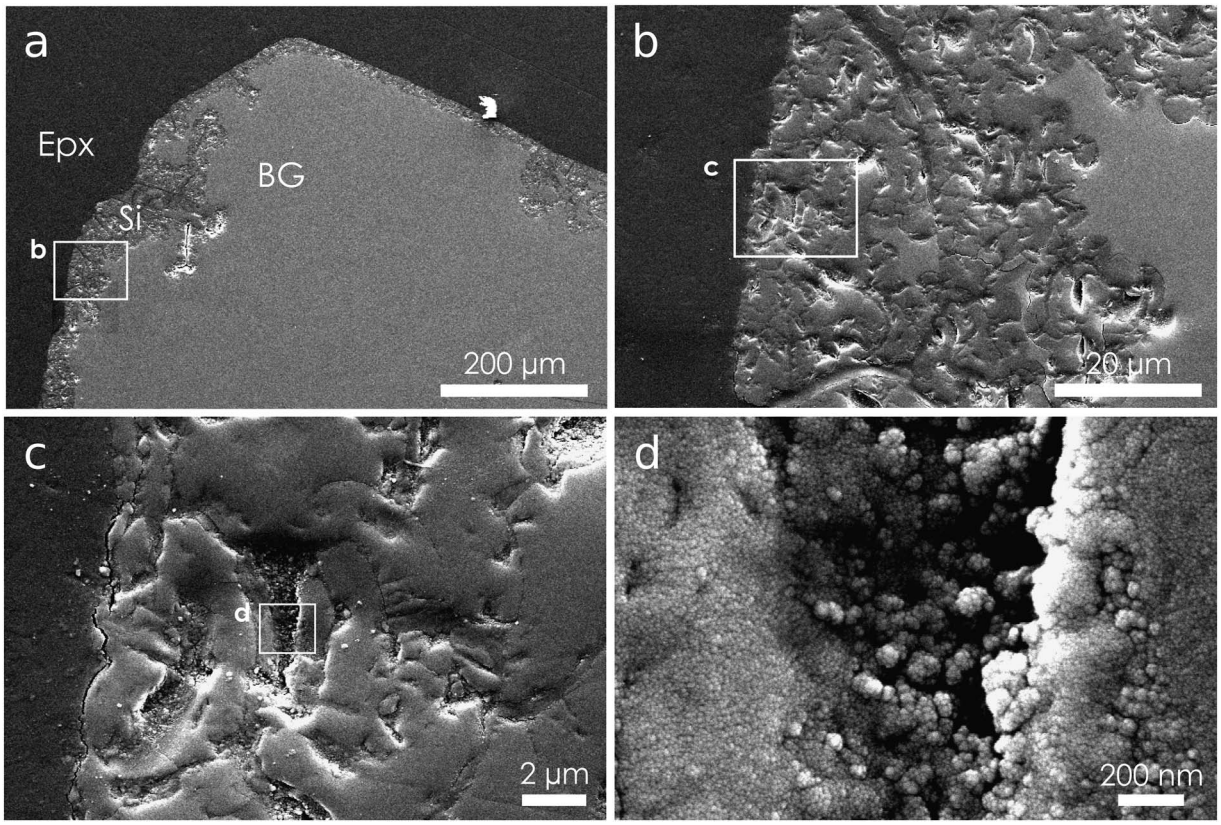

Figure 8. SE images of cross-section views of BAS101 grains exposed to starting pH ~1 acid solution. (a) Context image where Epx indicates epoxy, Si indicates a silica-enriched alteration phase, and BG indicates basalt glass. (b) Magnified to show fractured texture of Si-enriched layers. (c and d) Magnified to show spherical particulate in fractures.

due to the high abundance of Cr in the EDS data (Figures 3b and 3d). As far as we observed, the plagioclase quench crystals undergo the most significant Si-enrichment, which occurs within the boundaries of the plagioclase quench crystals, taking on their original shape. The glassy groundmass and the chromite crystals are affected to a lesser degree, and the pyroxene crystallites do not become enriched in Si during the experiments. Thus, acid alteration appears to be patchy, having permeated the entire grain, and produces silica-rich phases.

SE imaging highlights the highly fractured nature of the Si-enriched areas and shows nanometer-scale particulate in the fractures (Figures 4a and 4b). The particulate could represent newly precipitated material, residue left behind as the original structure was destroyed during the leaching process or material that was formed and deposited as a result of polishing during sample preparation.

4.1.3. Basaltic Glass in Low pH Acid

In BSE imagery, the basaltic glass (BAS101) samples exposed to starting pH ~1 acid exhibit continuous, relatively dark (low Z) alteration layers around the perimeter of the grains (Figure 5a). The layers exhibit conchoidal fracturing (Figures 5a and 5b) and vary in thickness from several to tens of microns, though the thicknesses could be overestimated if the grain surface is not normal to the polished surface. While the alteration predominantly occurs around the perimeter of the grains, it can proceed inward along thin fractures and crystal boundaries, affecting plagioclase crystals (Figure 5a). EDS point analyses of the starting material, the alteration layer, and the interior of the altered basaltic glass grains are shown in Figure 6d. The alteration layer is composed of Si and O with minor traces of Al. The grain interior composition falls roughly within error of the composition of the starting material but does exhibit a slight enrichment in Si, Mg, and Na and depletion in Ca and Fe compared to the starting material (Figure 6d). Thus, the alteration of basaltic glass under low pH solutions forms relatively thick Si-enriched layers, while plagioclase crystals are affected to a lesser degree.

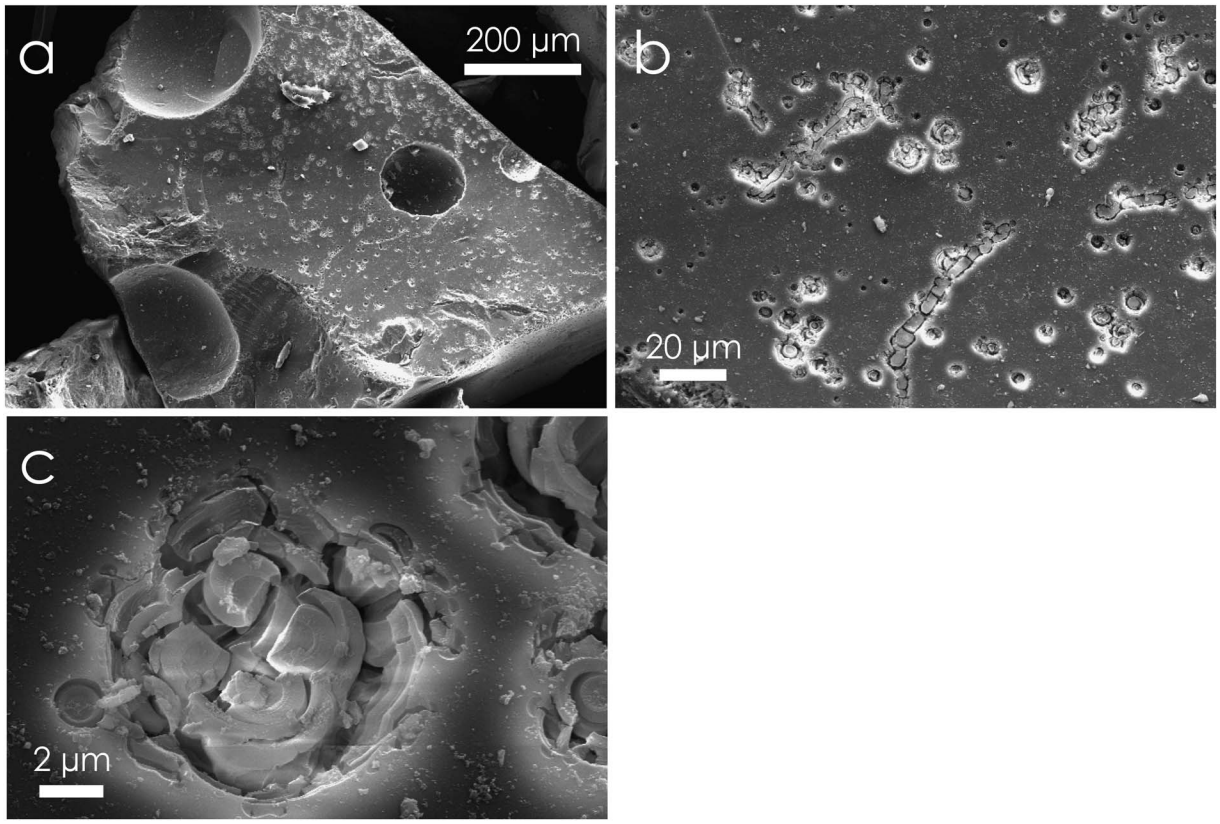

Figure 9. SE images of ICE170 grains weathered in starting pH ~3 acid solutions for 220 days. (a) Context image showing distribution of etch pits on surface of grain. We interpret the very large pits ~100–200 µm to be vesicles. (b) The same grain at greater magnification showing the pits and pit chains in greater detail. (c) Close-up of a pit.

The outer surfaces of the basaltic glass BAS101 grains weathered in starting pH ~1 acid solution display two main textures, a honeycomb-like texture and a highly fractured texture (Figure 7a). Overall, the honeycomb texture looks pockmarked and relatively interconnected, consisting of a series of ridges that bound nearly oval-shaped depressions with long axes ~10–30 µm in length (Figure 7b). Thin fractures occur throughout the honeycomb texture, forming predominantly in the depressions, but the locations of the fractures are otherwise unassociated with the geometry of the honeycomb texture. The grain surfaces beneath the honeycomb texture appear to be relatively smooth and rounded suggesting that this texture forms on natural surfaces (Figure 7a). The fractured texture consists of ubiquitous sharp and angular cracks, making the region appear very brittle (Figure 7c). Large conchoidal fractures (~200 µm long) and angular facets can be see beneath the fractured texture indicating that this texture forms on surfaces that were broken during sample processing (Figure 7a). Similar to the Si-enriched zones in ICE170, the alteration layers of BAS101 are highly fractured with nanometer-scale particulate in the fractures (Figures 8–8d).

4.1.4. Glassy Basalt in Moderate pH Acid

Dissolution etch pits and pit chains appear on the surfaces of ICE170 grains weathered in starting pH ~3 acid solutions for 220 days (Figures 9a–9c). The pits range from ~1–10 µm in diameter, and the chains can reach ~60 µm in length. Larger circular depressions ($>$ ~100 µm) are interpreted as primary vesicles. The etch pits resemble collapse features, which suggests that they formed as a result of a dissolution process. When viewed in cross section in BSE imagery, the grains show some concave features along the edges of the grains that could be the etch pits (Figure 10a). Some of the concave features contain a material that is darker toned, indicating that the material has fewer heavy elements than the rest of the grain and is most likely enriched in Si (Figure 10b). Otherwise, point and line EDS analyses showed no elemental evidence for any phases other than basaltic glass, plagioclase, and pyroxene. The crystal grain boundaries look smooth and relatively unaltered when compared to those in the samples exposed to starting pH ~1 acid solution, and the overall

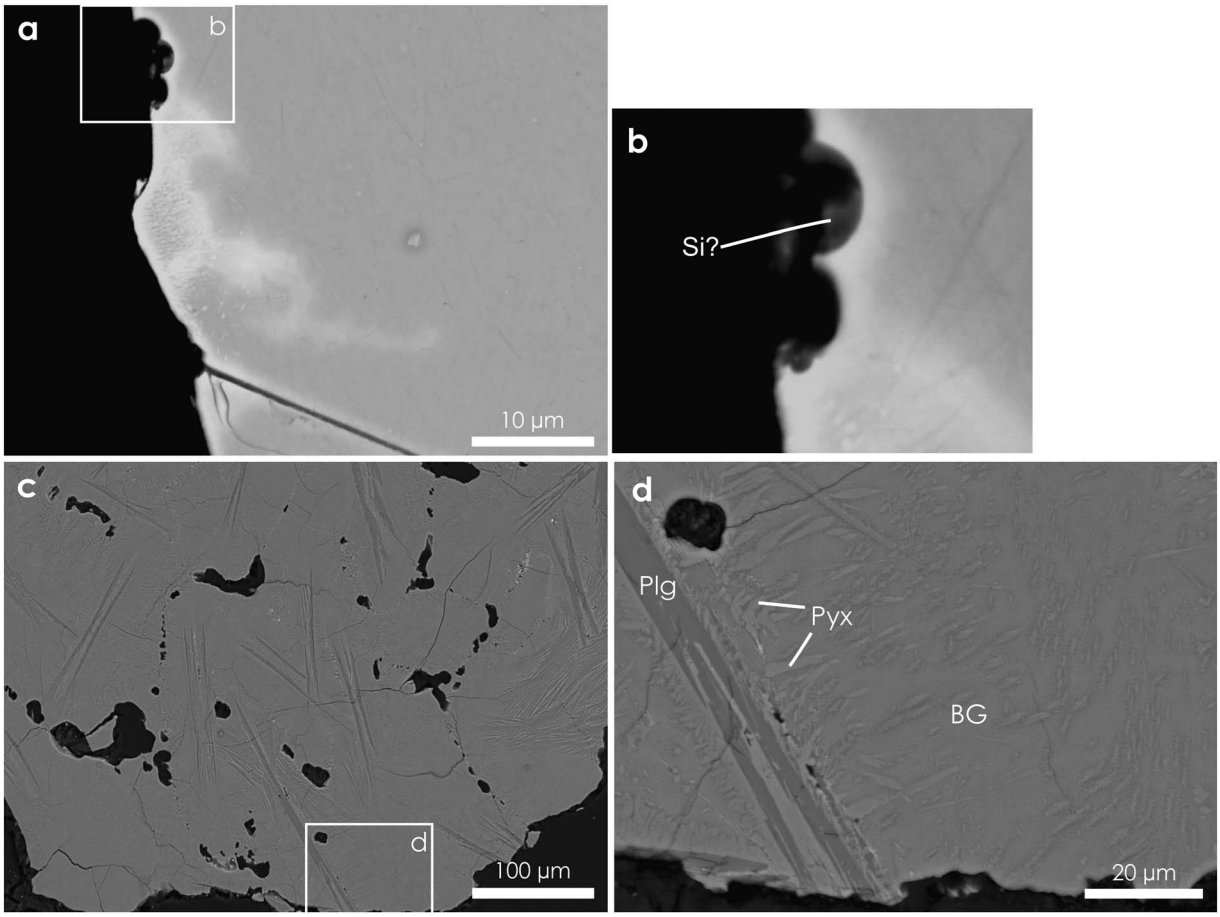

Figure 10. Cross-sectional BSE images of ICE170 grains weathered in starting pH ~3 acid solutions. (a) ICE170 grain that shows cross section through potential etch pits in the basalt glass (in white box). (b) Enlarged region from Figure 10a pointing out the possibly Si-enriched material in potential etch pits. (c) Context image with white box showing region enlarged in Figure 10d. (d) Enlarged region showing inside of grain with relatively unaltered plagioclase (Plg), pyroxene (Pyx), and basalt glass (BG). Note that there are bright regions inside (Figures 10a and 10b) and halos around much of the perimeter of the grain (Figure 10d) when viewed at higher magnification, which are due to charge buildup on the sample.

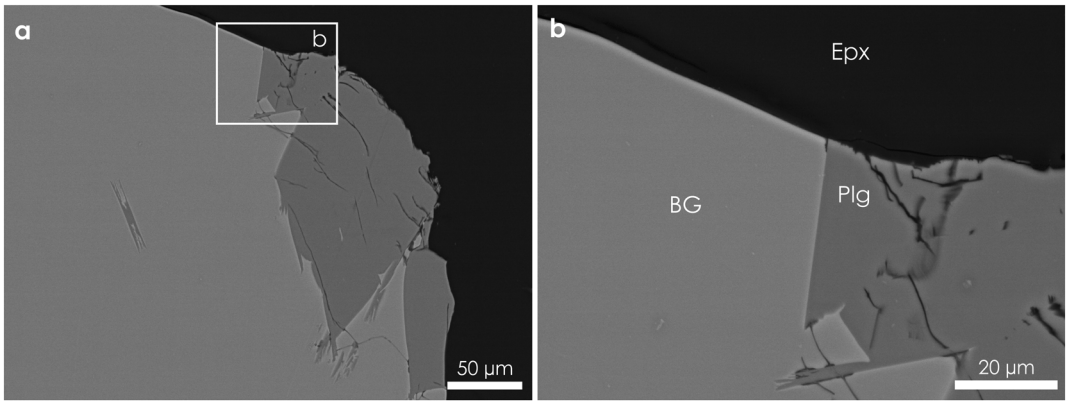

Figure 11. BSE images of BAS101 grains exposed to starting pH ~3 acid solutions. Epx indicates epoxy, Plg indicates plagioclase, and BG indicates basalt glass. (a) Context image of a cross section of a grain, and the white box shows the region enlarged in Figure 11b. (b) The interior is relatively unaltered at the micrometer scale, and there is no evidence for fluid interactions along crystal boundaries. The thin, bright halo around much of the perimeter of the grain when viewed at higher magnification (Figure 11b) is a result of charging on the sample.

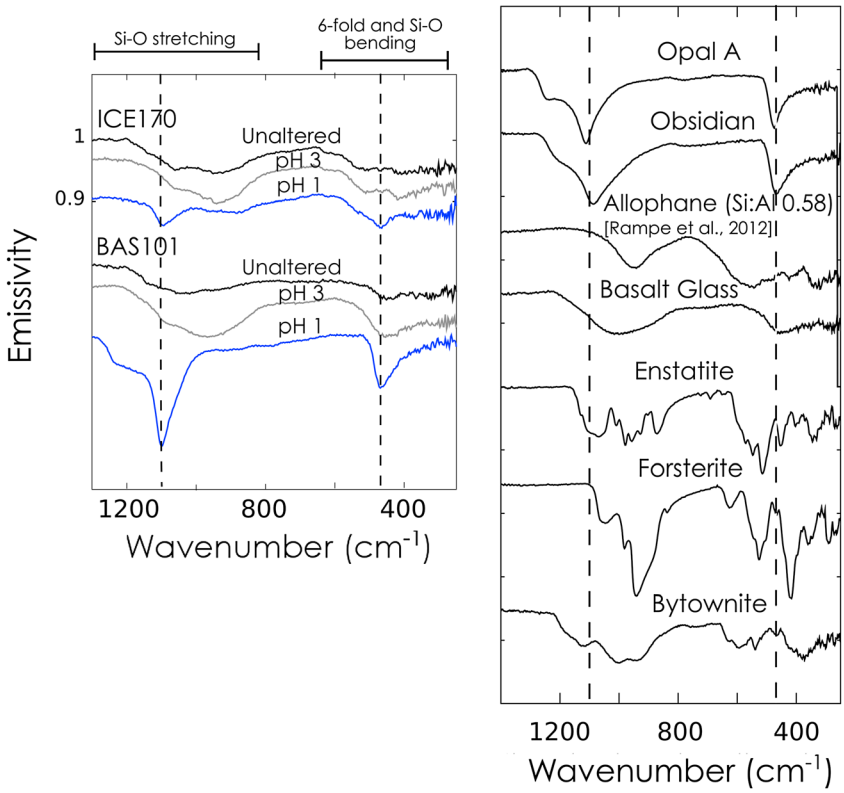

Figure 12. TIR spectra of basalt grains from these experiments. (left) Unaltered basalt grains (black), grains weathered in pH 3 acid (grey) and grains weathered in pH 1 acid (blue) for each experiment. Dashed lines mark the 1100 cm^{-1} and 465 cm^{-1} positions of the final emissivity minima for the basaltic glass samples weathered in starting pH ~1 acid solution. (right) TIR spectra of common minerals and phases from the Arizona State University online spectral library for reference. This figure is modified from *Horgan et al.* [2017].

morphology of the grains is very similar to that of the starting material (Figures 10c and 10d). The light-toned regions and halos that occur in and around the glassy basalt grains in Figures 10a and 10b are due to charging on the sample.

4.1.5. Basaltic Glass in Moderate pH Acid

The outer surfaces of basaltic glass BAS101 grains altered in starting pH ~3 acid solutions for 220 days show no obvious alteration textures when viewed in SE images, unlike their counterparts altered in starting pH ~1 acid solution. Additionally, there is no noticeable pitting on the grain surfaces as there was with ICE170 samples exposed to starting pH ~3 acid solutions. For the most part, when viewed in cross section (Figure 11a), the plagioclase phenocrysts crystal grain boundaries are sharp and unaltered, though the small (~1 μm) notches on the surface of the plagioclase crystal in Figure 11b could represent pitting. EDS point analyses show no evidence for elemental change from the starting material. The light-toned halos around the sample grains in Figures 11a and 11b are a resulting of charging on the sample.

4.2. TIR Spectra of Grains

A detailed analysis of the TIR spectra can be found in our companion paper [*Horgan et al.,* 2017], but the results from that study are summarized here. In general, the most extreme spectral changes are found in samples exposed to starting pH ~1 acid solution. When exposed to very low pH (pH ~1), both samples exhibit a narrowing of the Si-O stretching band (~800–1200 cm^{-1}) combined with a shift to a higher wave number, indicating an increase in abundance of more highly polymerized phases (Figure 12) [*White and Minser*, 1984; *Crisp et al.,* 1990; *Michalski et al.,* 2005]. The basaltic glass sample (BAS101) develops a very strong amorphous silica spectral signature that masks any signal from the underlying substrate. The spectral shape is very similar to that of opal-A, including 1220 cm^{-1} and 465 cm^{-1} features, but with a Si-O stretching emissivity minimum that shifts toward slightly lower wave number (~1100 cm^{-1}). The glassy basalt sample

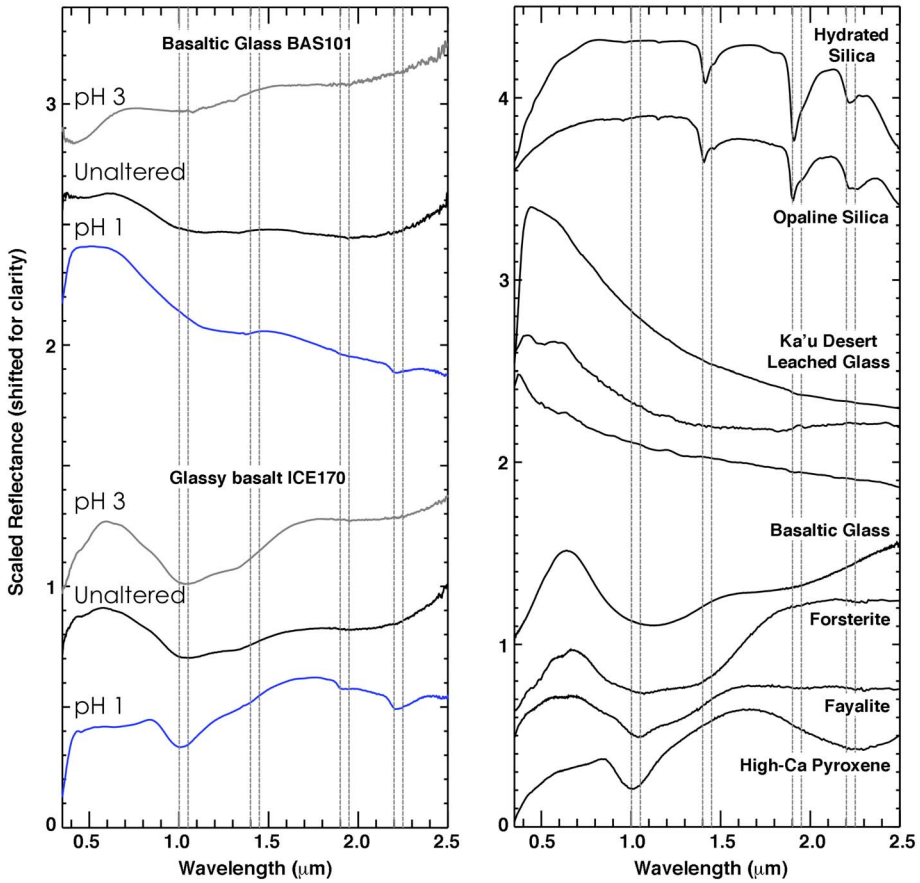

Figure 13. VNIR spectra of basaltic grains from these experiments. (left) Unaltered basaltic material (black), grains weathered in pH 3 acid (grey), and grains weathered in pH 1 acid (blue) for each experiment. Lines mark the positions of the most spectral change (1.0, 1.4, 1.9, and 2.2 μm). (right) VNIR spectra of common minerals and for reference. Lines are in the same positions as in the figure on the left.

(ICE170) exposed to starting pH ~1 acid solution also develops an amorphous silica spectral signature with features near 1090 cm^{-1} and 465 cm^{-1} but does not develop a 1220 cm^{-1} feature. Additionally, less polymerized phases (e.g., pyroxene and olivine) are detected in the altered ICE170 spectrum based on the absorption features near 950 cm^{-1}, suggesting that the optically active part of the sample is a mixture of silica-rich alteration phases and unaltered material.

In contrast, when exposed to starting pH ~3 acid solutions, both the glassy basalt and basaltic glass samples show emissivity minima shifts toward lower wave numbers in the Si-O stretching region, which suggests increased disorder (Figure 12).

4.3. VNIR Spectra of Grains

A detailed analysis of the VNIR spectra can be found in our companion paper [*Horgan et al.*, 2017], but the results from that study are summarized here. Similarly to the TIR, the most extreme spectral changes in the VNIR occur when samples are exposed to starting pH ~1 acid solution (Figure 13). Changes during alteration include both the weakening of the iron bands (1 and 2 μm) overall, as well as the strengthening of pyroxene absorptions at the expense of olivine absorptions. Additionally, we observe the appearance of narrow absorption bands near 1.4, 1.9, and 2.2 μm, consistent with the deposition of alteration minerals that include silica and hydrated glass. The appearance of these bands correlates well with models of increased high-silica phases in TIR spectra. Lastly, we observe the development of strong blue spectral slopes (decreasing reflectance with increasing wavelength) with concave up and/or linear shapes. These spectral slopes only occur in the basaltic glass sample, and their appearance is correlated with the appearance of a shoulder at 1220 cm^{-1} in the thermal IR spectra of these samples.

In contrast, samples altered under starting pH ~3 solutions show very little spectral evidence for alteration. VNIR spectra of the glassy basalt samples (ICE170) are virtually unchanged after exposure to pH ~3 solutions, while the basaltic glass sample (BAS101) develops weak absorption edges in the visible and red spectral slopes (increasing reflectance with increasing wavelength), both potentially consistent with the enrichment of amorphous ferric iron. However, no oxides are detected in the BSE images or in the TIR spectra of this sample, and so any oxide coating must be very thin (nanometers thick).

5. Discussion

5.1. Effects of Crystallinity on Alteration Texture and Morphology

Crystal grain boundaries are effective pathways that enable fluid to infiltrate a sample [e.g., *Jonas et al.,* 2014]. Thus, low pH alteration fluids are able penetrate the interiors of the more crystalline samples (ICE170), developing patches of altered material throughout the sand-sized grains. The glass samples (BAS101), on the other hand, have fewer phenocrysts, and so there are fewer zones of weakness for the solution to penetrate. In the absence of crystal grain boundaries, the acid is forced to attack the perimeter of the grain, propagating inward through the conchoidal fracturing of the altered material as a result of volume change with phase change (Figure 5b). The volume change appears to be negative because the silica-rich areas are slightly recessed from the unaltered interior (Figure 5b). We mostly attribute the observed fractures to volume change with alteration, but the desiccation of a hydrated silica-rich alteration phase in the SEM vacuum environment could also form fractures. However, we did not observe fractures opening over time as the samples were analyzed and so we expect desiccation to play a minor role in the resulting fracture widths. Thus, crystal grain boundaries allow for a more heterogeneous interior alteration, and fewer crystal grain boundaries promote the development of a continuous alteration layer.

The materials altered in the weaker (pH 3) acid also show differences based on crystallinity. The partially glassy basalt (ICE170) samples develop etch pits on the surface of the grains, which indicate that some dissolution is taking place. The basaltic glass grains, on the other hand, do not have any etch pits and are relatively smooth. Etch pits easily form on crystallographically controlled surface features, such as defects [*Berner and Holdren*, 1977; *Berner*, 1978], of which an amorphous, glassy surface might have fewer.

5.2. Effects of pH on Alteration Morphology

The differences between basaltic materials altered in low versus moderate pH acid solutions are extreme. Materials exposed to moderate pH (~3) acid solutions show little sign of alteration to both the interior and exterior of the sample grains. On the other hand, materials exposed to low pH (~1) acid solution exhibit alteration at the surface and throughout the grains and have silica-rich surface altered layers and zones.

While dissolution is surely taking place, neither of the samples exposed to starting pH ~3 acid solutions show evidence for large-scale phase changes or alteration, consistent with the lack of spectral change in the VNIR. The glassy basalt (ICE170) samples do form surficial etch pits, the size and shape of which resemble pits formed on basaltic glass samples etched in HF acid [*Fisk et al.,* 2013]. Additionally, the etch pits formed in our experiments contain small deposits of a material that is potentially silica rich. However, no hydrated silica phases are detected in the VNIR or TIR spectra so the total volume of silica-rich material must be small. The general paucity of alteration phases found on materials exposed to moderate acid solutions suggests that most of the dissolved material remains in solution long enough to be flushed away as the acid baths are refreshed or that precipitated phases are loosely bound to the grains so that they are easily removed as the samples are washed. While the presence of a silica-rich alteration layer could indicate either congruent or incongruent dissolution, the absence of such a layer on both samples exposed to more moderate pH fluids suggests that no leaching (incongruent dissolution) has taken place.

In contrast, the basaltic materials exposed to starting pH ~1 acid solution exhibit significant evidence for alteration. Both samples form silica-rich layers or zones, confirming VNIR and TIR detections of amorphous silica-rich phases. This indicates that a highly acidic environment is more conducive for forming silica-enriched weathering products than a moderate pH environment. The silica-rich alteration layers and zones in both samples are associated with fractures. The fractures either formed as a result of volume change as the original material was replaced with the silica-rich material, as a result of postalteration environmental factors (e.g., through desiccation of a hydrated alteration phase or plucking of the softer alteration phases

during sample polishing), or some combination of both. As noted in section 5.1, the conchoidal fracturing visible in cross section most likely formed during alteration but has possibly undergone some additional opening due to desiccation. It is unlikely that this texture formed during sample polishing because of the close association with the reaction boundaries.

The basaltic glass sample (BAS101) altered under low pH fluids also developed fractured terrain and the honeycomb textures (Figure 7a) on the surfaces of the grains that were not subject to any postalteration sample preparation techniques. The fractured terrain is similar to fractures on laboratory altered basaltic glass described by *Gislason and Oelkers* [2003]. They suggested that this texture was due to (1) preferential dissolution along weak areas incurred when the glass was initially cooling, (2) effects of drying the grains after the experiments, and/or (3) spalling of an altered layer precipitated on the surface. In this study, the fractured textures appear on the angular sides of the grains, which most likely represent surfaces formed when the glass was being ground to sand sized particles. Therefore, it is likely that the fractured alteration texture represents dissolution along weak areas incurred during sample processing.

The honeycomb textures found on the surfaces of the basaltic glass samples exposed to low pH (~1) alteration fluids are not so easily explained as there are few textures described in the literature that are of comparable morphology. *Berner and Holdren* [1977] also describe a honeycomb texture found on naturally weathered feldspar crystals, but these are coalesced steep walled, rectangular to almond-shaped etch pits, differing greatly from the shallow, generally oval-shaped depressions found in this study. However, *Berner and Holdren* [1977] also show a pitted feldspar crystal coated with desiccated clay minerals, and the depressions are slightly shallower, more diffuse, and irregularly shaped. This surface more closely resembles the honeycomb texture found on our basaltic glass samples. Therefore, it is possible that the depressions that make up the honeycomb texture found in our study are etch pits on the surface of the glass that are coated with a silica-rich alteration layer permeated by fine ($<$ ~1 μm) fractures related to desiccation. The depressions in the honeycomb terrain are roughly the same scale as the conchoidal fractures seen in cross section (Figure 5b) and, thus, could be the surface expression.

At very low pH, the order of solubility is usually basaltic glass $>$ olivine $>$ plagioclase $>$ pyroxene [*Hausrath et al.,* 2008]. At starting pH ~1, this simple model works when applied to our basaltic glass sample (BAS101) in which we see the preferential alteration of glass over plagioclase phenocrysts in the BSE images as well as in the TIR spectral data. When applied to the more crystalline sample (ICE170), the model works in that plagioclase is preferentially lost relative to pyroxene as indicated by BSE imaging, and VNIR, and TIR spectroscopy. Yet BSE images clearly show that plagioclase is being preferentially lost relative to basaltic glass. In general, ICE170 has more quench crystals than the basaltic glass samples, which have a greater surface area to volume ratio making them more susceptible to weathering. Thus, we hypothesize that the favorable dissolution of plagioclase over basaltic glass in ICE170 is related to crystal grain size and geometry.

It should be noted that *Tosca et al.* [2004] found that highly acidic weathering of crystalline basalt favored deposition of sulfates and amorphous silica at a persistently acidic pH, while moderately acidic weathering released enough solutes to buffer the solution to higher pH and then precipitated iron oxides. However, neither ICE170 nor BAS101 altered in starting pH ~1 acid solution developed evidence of sulfates, and neither of the samples exposed to starting pH ~3 acid solutions developed iron oxides. It is possible that these phases formed but were removed when the grains were gently washed.

In summary, the differences between materials altered in low versus moderate pH acid solutions are significant. Materials exposed to moderate pH (~3) acid solutions show little sign of alteration to both the interior and exterior of the sample grains, indicating that the environment is more conducive for the transportation of solutes away from the samples. On the other hand, materials exposed to low pH (~1) acid solution exhibit alteration at the surface and throughout the grains and have layers and zones of amorphous silica-rich phases indicating that the environment must be conducive for the retention or precipitation of amorphous silica.

5.3. Effects of Silica-Rich Alteration Morphology and Chemistry on Thermal Infrared Spectra

The wave number of the major Si-O emission feature in the TIR is proportional to the degree of polymerization of the silicate structure. The degree of polymerization of a silicate glass or amorphous substance is a function of the number of shared, or bridging oxygen atoms per network-forming tetrahedra [*Henderson*,

2005; *Calas et al.,* 2006], which is affected by the abundance of network-modifying cations (e.g., Na^+, K^+, Mg^{2+}, and Ca^{2+}) and H_2O [*Henderson*, 2005; *Michalski et al.,* 2005; *Calas et al.,* 2006]. Network-modifying cations and H_2O molecules cause a structure to depolymerize by forcing openings within the structure and creating charge imbalance which are neutralized with nonbridging oxygen atoms [*Farnan et al.,* 1987]. Al^{3+} and Fe^{3+} substitution in network-forming tetrahedra can also decrease polymerization due to longer bond distances as a result of the increased ionic radius relative to Si^{4+}. The substitution also introduces a charge imbalance that is neutralized with network-modifying cations, which further depolymerizes the structure [*Henderson*, 2005; *Michalski et al.,* 2005; *Calas et al.,* 2006].

EDS measurements of the silica-enriched regions and layers in ICE170 and BAS101 samples exposed to starting pH ~1 acid solution indicate that the phases are not pure silica. The measurements detect small concentrations of Al^{3+} (some potentially in tetrahedral coordination) and Ca^{2+} (a network modifying cation). Additionally, VNIR spectra indicate that the silica-enriched phases are hydrated. Therefore, it is likely that the structure is less polymerized than a pure hydrated silica phase, such as opal-A. Indeed, the locations of the Si-O stretching emission features of our altered samples at ~1090 and 1100 cm^{-1} are at lower wave numbers than that of opal-A (which has an Si-O stretching feature ~1115 cm^{-1}).

In the thermal infrared, silica-enriched zones and layers have different spectral effects. The more crystalline samples (ICE170) exposed to low pH (~1) acid solution have heterogeneously altered perimeters consisting mostly of Si-enriched zones, altered basaltic glass, and other primary minerals such as chromite. Correspondingly, the spectra appear as mixtures of high-silica phases (~1090 cm^{-1} and 465 cm^{-1} emissivity features) and mafic minerals (~950 cm^{-1} emissivity feature). The spectral shape of altered ICE170 is similar to that of crystalline basalt coated with very thin (~1 μm) layers of pure colloidal silica [*Kraft et al.,* 2003], although the Si-O stretching feature of altered ICE170 is at slightly lower wave number than that of the pure silica coating, as discussed above.

On the other hand, thick (~10–100 μm) continuous layers on the glass samples (BAS101) exposed to starting pH ~1 acid solution effectively mask any spectral signal from the underlying substrate. The resulting spectrum only exhibits features associated with amorphous silica-rich phases (1100 cm^{-1}, 465 cm^{-1}, and a 1220 cm^{-1} shoulder). The altered BAS101 spectral shape resembles that of pure silica coatings $>$ ~6 μm thick on crystalline basalt [*Kraft et al.,* 2003], but with a Si-O stretching feature slightly shifted to lower wave number.

The penetration depth for spectral measurements is dependent on both the wavelength of light, and the optical properties of the materials. Our results, along with those of *Kraft et al.* [2003] and *Minitti et al.* [2007], indicate that the absorption coefficient of the coating material is very important when considering the penetration depth of the measurement. Silica has a very high absorption coefficient so that layers $>$ ~3 μm thick can completely obscure the underlying basaltic materials, effectively decreasing the penetration depth. Therefore, while making up a relatively small percentage of the total volume of material, silica coatings and layers can cause the abundance of silica in a sample to be grossly overestimated. Samples with heterogeneous silica-rich alteration textures do not have this spectral effect. This point has important implications for the interpretation of TIR remote sensing data from planetary surfaces.

The 1220 cm^{-1} shoulder feature is present in the TIR spectrum of the basaltic glass samples exposed to low pH acid but is absent in the TIR spectrum of the glassy basalt from this study. This feature is also present in the TIR spectra of many silica-rich glasses and silica-rich amorphous alteration phases and represents one of two states of the SiO_2 asymmetric stretching mode [*Minitti et al.,* 2007]. It is unknown what would cause the 1220 cm^{-1} shoulder feature to be absent in TIR spectra when silica-rich materials are otherwise being detected. *Kraft et al.* [2003] found that the feature was missing from the TIR spectra of basalt with silica coatings $<$ ~3 μm thick, and *Crisp et al.* [1990] noted that the feature was absent in spectra from lava flow less than 50 years old. These results indicate that coating thickness is an important factor; suggesting that the spectral feature only becomes present when the silica-rich coating or layer is of sufficient thickness or when silica-rich material makes up a large enough percentage of the volume of material being measured. However, *Minitti et al.* [2007] found that one sample with ~2–3 μm thick silica-rich coatings/layers (MUO, Mauna Ulu) exhibited the 1220 cm^{-1} spectral shoulder, while another sample with generally thicker coatings/layers (~5–7 μm; MIY, Mauna Iki) did not. Thus, there are most likely other factors controlling the presence or absence of the

1220 cm^{-1} shoulder feature. Other suggested factors include material porosity [*Ruff et al.,* 2011] and viewing angle [*Almeida*, 1992; *Ruff et al.,* 2011].

5.4. Effects of Silica-Rich Alteration Morphology on Visible to Near-Infrared Spectra

As with the thermal infrared wavelength measurements, the different silica-rich alteration textures formed in both materials under low pH fluids have distinct effects on the VNIR spectra. The heterogeneous alteration textures found in the glassy basalt sample (ICE170) are exhibited as both hydrated silica and mafic mineral spectral features in the VNIR, consistent with the TIR measurements. However, the spectrum does not exhibit any features that would uniquely identify this heterogeneous alteration morphology from a physical mixture of basaltic minerals and hydrated silica.

In contrast, the continuous silica-rich alteration layer on the basaltic glass sample (BAS101) completely masks any spectral signature from the underlying basaltic glass substrate. The VNIR spectrum develops hydrated silica spectral features as well as a strong concave up slope (greater blue slope at shorter wavelengths) at the expense of any mafic mineral spectral signatures. The concave up slope shape has been attributed to leached rinds formed on natural glass samples during acid leaching [*Minitti et al.,* 2007; *Horgan and Bell*, 2012; *Horgan et al.,* 2017]. While the SEM results from this study confirm the presence of silica-enriched layers on the basaltic glass samples, it is not certain that the layers are leached rinds, as will be discussed in section 5.5.

5.5. Comparison to Natural Silica-Enriched Surface Alteration Layers

The samples exposed to starting pH ~1 acid solution show some morphologic and spectral similarities to naturally altered Hawaiian basaltic glass samples. All of the naturally altered basaltic glasses samples studied by *Minitti et al.* [2007] exhibit silica-enriched surface alteration layers, similar to our basaltic glass sample, and none show alteration textures extending toward the interior of the samples as we see in our glassy basalt sample. The natural samples most spectrally similar to our laboratory samples in the thermal infrared are not necessarily similar to our samples in the near infrared. This is most certainly a result of differences in alteration morphology, sensing depth, and the variety of thin surficial oxide and sulfur-rich coatings on the natural samples that are not seen in our laboratory samples.

The natural samples most spectrally similar to our laboratory samples in the thermal infrared all have continuous, silica-rich layers, with marble-texture, capped with thin, discontinuous Ti and Fe oxides and sulfur-rich phases. The silica-rich layers on the natural samples appear similar in porosity to the silica-enriched layers and zones of our laboratory samples, but none have the conchoidal fracturing found in the layers on our basaltic glass samples. Additionally, none of our samples have evidence for oxide or sulfur-rich capping layers, which could have been washed away during sample processing. Regardless, the spectral similarities suggest that thin oxide and sulfur-rich capping layers must have very little effect on the thermal infrared spectrum.

Our basaltic glass samples exposed to starting pH ~1 solution are most spectrally consistent with samples acquired from a basalt flow at Kilauea (KW) and from the Mauna Iki flow field along the Kilauea SW rift zone (MIO). BSE imagery shows that these natural samples have thick (10–35 μm and 20–80 μm, respectively) silica-rich layers, and their TIR spectra are completely dominated by an amorphous silica-rich phase displaying features at ~1100 cm^{-1}, 470 cm^{-1}, and a shoulder feature ~1220 cm^{-1}. In contrast, the glassy basalt samples exposed to starting pH ~1 acid solution look most spectrally similar in the thermal infrared to a naturally altered sample collected from a lava channel at Mauna Ulu (MUO). This sample has much thinner (~2–3 μm) silica-rich layers, and the TIR spectrum displays a mafic feature at ~880 cm^{-1} and silica spectral features at ~1100 cm^{-1} and 470 cm^{-1}. This observation supports our hypothesis that thin layers and heterogeneous alteration spectra combine more linearly with the substrate spectra than thicker alteration layers, so that both mafic and silica spectral features are visible in the resulting thermal infrared spectral shape. It should be noted that unlike our glassy basalt sample, the TIR spectrum of the MUO sample has a weak absorption near 1250 cm^{-1}, which could be the initiation of a 1220 cm^{-1} shoulder feature.

In the VNIR, the spectral similarities between naturally altered Hawaiian basaltic glass samples and our laboratory samples altered under strongly acidic solutions are less apparent. This is most likely a result of small-scale variations in morphology and composition in the natural samples that affect the shorter wavelength measurements to a greater extent than the longer wavelength TIR measurements.

All of the naturally altered samples are quenched glassy exteriors of basaltic flows that contain few phenocrysts, and none of the naturally altered basaltic glass samples exhibit alteration morphology similar to our glassy basalt sample. Additionally, all of the naturally altered samples exhibit blue, and sometimes concave up slopes in the VNIR. This feature is missing from our altered glassy basalt sample (ICE170), and so none of the natural samples have comparable spectra.

On the other hand, our basaltic glass sample altered in low pH fluids does have silica-rich alteration layers and a VNIR spectrum exhibiting a concave up blue spectral slope, and so this sample is more similar spectrally to the naturally altered basaltic glass samples. This supports our hypothesis that basaltic glasses are more likely to form silica-rich coatings or layers, which introduce a blue, and sometimes concave up, slope to the VNIR spectrum. It is interesting to note that none of the natural samples exhibit 2.2 μm features associated with silica, and the VNIR spectra of samples that display concave up blue spectral slopes are otherwise smooth and relatively featureless.

5.6. Possible Formation Mechanisms for Silica-Enriched Layers and Zones

Here we speculate about the formation mechanisms for the silica-enriched alteration textures based on chemical, morphologic, and spectral observations. None of the silica-enriched samples show layers that appear to have been accreted, and none contain detritus or other mineral fragments. This allows us to eliminate a silica coating formation mechanism, as defined in section 2.3. Thus, the surface altered layers and zones must either be a result of leaching or dissolution-reprecipitation.

Most of the alteration textures of the glassy basalt sample (ICE170) are consistent with dissolution-reprecipitation mechanisms. For example, plagioclase quench crystals are replaced by the silica-rich phase, and replacement is thought to occur through dissolution-reprecipitation mechanisms [*Putnis and Putnis*, 2007; *Hellmann et al.,* 2012; *Ruiz-Agudo et al.,* 2014]. Additionally, it is likely that some of the fractures and porosity of the Si-enriched regions resulted from the molar volume differences between parent and product [*Pollok et al.,* 2011]. The composition of the silica-enriched regions is consistent with observed compositions of either leached or precipitated layers [*Hellmann et al.,* 2012]. The average compositions of the altered glass regions seem more consistent with a leaching mechanism. However, the feathered textures in Figure 2d could be submicron scale interlacing of two end-member compositions: an unaltered basaltic glass and precipitated Si-enriched regions. Due to the micron-sized spot size of the EDS measurement, such a texture would create an average composition consistent with a silica-enriched basaltic glass, but the texture would be more consistent with a dissolution-reprecipitation mechanism.

The composition of the Si-enriched layers found on the basaltic glass samples (BAS101) altered in pH 1 acid solution is consistent with that of both leached and precipitated layers. However, the silica-enriched layers are much thicker than most leached rinds and are more similar to thicknesses of precipitated layers. The layers are highly porous and fractured, potentially resulting from volumetric changes during replacement [*Pollok et al.,* 2011; *Chemtob and Rossman*, 2014], and the plagioclase crystal in Figure 5a is starting to be replaced with silica. Replacement is indicative of dissolution-reprecipitation mechanisms.

Therefore, we conclude that the silica enrichment of basaltic materials exposed to low pH acid solutions results from dissolution-reprecipitation mechanisms and that silica-rich precipitated layers form selectively on basaltic glass. Our conclusions are consistent with those of *Chemtob and Rossman* [2014] who observed natural silica-rich layers on Hawaiian basaltic materials and determined that silica-rich alteration layers formed selectively on surfaces with glassy surface layers. Additionally, they concluded that the layers formed through the acidic dissolution of near-surface basalt, followed by in situ precipitation of amorphous silica.

5.7. Implications for Mars

Any phase proposed to exist on the Martian surface in great abundance ($>$ ~5–15%) [*Christensen et al.,* 2001] must agree with both near-infrared and thermal infrared data sets. Our results show that the spectral features of acid altered basaltic materials can be diagnostic of physical alteration textures, which are strongly controlled by both the pH of the alteration fluids and the crystallinity of the starting material. Alteration of basaltic materials under moderately strong acidic fluids (pH $\geq$ ~3) in an open system will not produce diagnostic spectral features related to the alteration of the substrate alone (although this will produce secondary minerals) [e.g., *Yant et al.,* 2016]. Whereas alteration under strongly acidic fluids (pH $<$ ~3) in an open system enables the precipitation of silica-rich phases that are easily detected in both TIR and VNIR

spectra. More crystalline basaltic materials exhibit heterogeneous alteration textures that are manifested in the VNIR and TIR spectra as mixtures of mafic minerals with a silica-rich phase. On the other hand, basaltic glass materials form silica-rich alteration layers that completely obscure the spectrum of the underlying substrate and give the VNIR spectra a diagnostic concave up blue slope that is not observed in spectra of silica coatings.

Large regions of the northern lowland plains of Mars, including Siton Undae and much of Acidalia and Utopia Planitiae, have thermal infrared spectra that are modeled with high abundances of high silica phases (15–20%) [*Bandfield*, 2002]. The same regions on Mars exhibit distinct concave up and blue near-infrared spectral slopes [*Horgan and Bell*, 2012; *Horgan et al.,* 2017]. Thus, basaltic glass altered under strongly acidic fluids is consistent with both VNIR and TIR spectral data from the Martian surface.

Our companion paper demonstrated that the thermal infrared spectra of basaltic glasses altered in starting pH ~1 acid solution are modeled with ~65–70% high silica phases [*Horgan et al.,* 2017], which are abundances far too high to be consistent with modeled abundances for the northern lowland plains. This suggests that the surface is actually a mixture of silica-rich alteration layers on basaltic glass and primary phases, an interpretation that is consistent with previous VNIR mapping studies from the northern polar region [*Tanaka et al.,* 2008; *Horgan and Bell*, 2012].

We do not think that given enough time, basaltic glass exposure to more moderate acid fluids (~pH 3) would eventually attain the same level of alteration as that observed at lower pH, because there is little evidence for silica-rich phase precipitation on our samples even after 220 days of exposure to acid. This suggests that large regions on Mars, particularly in the northern polar sand seas, are consistent with alteration by very acidic fluids. Acidic fluids have long been proposed as alteration fluids for the surface of Mars [e.g., *Clark et al.,* 1979; *Settle*, 1979; *Burns and Fisher*, 1993; *Banin et al.,* 1997; *Hurowitz and McLennan*, 2007]. Additionally, it has been shown that small volumes of near-neutral pH water could rapidly acidify upon exposure to oxidizing Martian surface conditions (atmospheric O_2 or photooxidation by ultraviolet radiation) [*Hurowitz et al.,* 2010] or through reactions with volcanic aerosols [*Niles and Michalski*, 2009]. Thus, it is possible that fluids derived from ice or snowmelt at low water/rock ratios are capable of obtaining the acidity needed to form alteration layers on basaltic glass.

In summary, we find that large regions of the Martian surface including Siton Undae and much of Acidalia and Utopia Planitiae are spectrally consistent with the alteration of basaltic glass in a low pH environment in both the VNIR and thermal infrared data but are not consistent with crystalline basalt altered in low pH fluids. Thus, it is highly likely that some amount of glass-forming volcanism (e.g., phreatomagmatic) has taken place on the Martian surface, and the glassy deposits were later altered at low water/rock ratios with highly acidic fluids. Detailed thermal infrared analysis of the northern polar region using the spectra of acid-altered basaltic materials from *Horgan et al.* [2017] would help support this hypothesis.

6. Conclusions

1. Alteration morphology is strongly controlled by pH of alteration solution and texture of starting material.
2. Only pH $<$ 3 acid is strong enough to create silica-enriched layers/zones in basaltic materials that are detectable in the visible to near infrared or thermal infrared.
3. Silica-enriched layers/zones appear to result from a dissolution-reprecipitation mechanism.
4. Crystal grain boundaries provide pathways for fluid to enter the interior of a grain, creating patchy alteration throughout the particle.
5. Less crystalline material has fewer pathways for the fluid to penetrate along, and so alteration is restricted to the exterior of the grain, creating a thick surface altered layer around the particle.
6. Grains with patchy alteration exhibit VNIR and TIR spectral features associated with both the substrate and the silica-rich alteration phases, while grains with continuous silica-enriched surface altered layers exhibit only hydrated silica VNIR and TIR spectral features. Additionally, continuous silica-enriched surface altered layers are distinct in the VNIR due to a concave up blue spectral slope.
7. Only basaltic glass samples exposed to low pH fluids (~1) have VNIR and TIR spectra that are consistent with the low-albedo northern lowland regions on Mars
8. Explosive volcanism likely took place, creating volcanic glass deposits that were later altered in low water: rock ratios by highly acidic fluids.

Acknowledgments
This work was funded in part by the NASA 2001 Mars Odyssey THEMIS project (Jet Propulsion Laboratory contract 1228404 through Arizona State University) and by the Arizona State University Exploration Postdoctoral Fellowship. This manuscript was significantly improved by the comments and suggestions of Steven Chemtob and an anonymous reviewer. We thank the Arizona State University LeRoy Eyring Center for Solid State Science and John M. Cowley Center for High-Resolution Electron Microscopy for use of their facilities for the laboratory portion of this work, the Natural Sciences and Engineering Research Council of Canada, the Canadian Space Agency, the Canada Foundation for Innovation, the Manitoba Research Innovations Fund, and the University of Winnipeg for supporting the establishment and operation of the Planetary Spectrophotometer Facility. We also thank Diana Convey for assistance with SEM sample preparation, Zhenquan Liu and Jinping Hu for technical support using the SEM, Jessica Stromberg for assisting with the acid dissolution experiments, and Stan Mertzman for his analysis of the samples. Tom Sharp, Michael Kraft, and Steve Ruff provided valuable insight that vastly improved this work. All visible and near-infrared spectra presented in this work are available from the University of Winnipeg: http://psf.uwinnipeg.ca, and all thermal infrared spectra are available from the TES spectral library: http://speclib.asu.edu. All EDS semiquantitative data can be found in table formats in the supporting information.

References

Abrams, M., E. Abbott, and A. Kahle (1991), Combined use of visible, reflected infrared, and thermal infrared images for mapping Hawaiian lava flows, *J. Geophys. Res.*, *96*, 475–484, doi:10.1029/90JB01392.

Almeida, R. M. (1992), Detection of LO modes in glass by infrared reflection spectroscopy at oblique incidence, *Phys. Rev. B*, *45*(1), 161–170, doi:10.1103/PhysRevB.45.161.

Bandfield, J. L. (2002), Global mineral distributions on Mars, *J. Geophys. Res.*, *107*(E6), 5042, doi:10.1029/2001JE001510.

Bandfield, J. L., V. E. Hamilton, and P. R. Christensen (2000), A global view of Martian surface compositions from MGS-TES, *Science*, *287*(5458), 1626–1630.

Banfield, J. F., G. G. Ferruzzi, W. H. Casey, and H. R. Westrich (1995), HRTEM study comparing naturally and experimentally weathered pyroxenoids, *Geochim. Cosmochim. Acta*, *59*(1), 19–31, doi:10.1016/0016-7037(94)00372-S.

Banin, A., F. X. Han, I. Kan, and A. Cicelsky (1997), Acidic volatiles and the Mars soil, *J. Geophys. Res.*, *102*, 13,341–13,356, doi:10.1029/97JE01160.

Belkorissat, R., A. E. D. Kadoun, M. Dupeyrat, B. Khelifa, and C. Mathieu (2004), Direct measurement of electron beam scattering in the low vacuum SEM, *Microchim. Acta*, *147*(3), 135–139, doi:10.1007/s00604-004-0182-x.

Berger, G., J. Schott, and M. Loubet (1987), Fundamental processes controlling the first stage of alteration of a basalt glass by seawater: An experimental study between 200° and 320°C, *Earth Planet. Sci. Lett.*, *84*(4), 431–445.

Berner, R. A. (1978), Rate control of mineral dissolution under Earth surface conditions, *Am. J. Sci.*, *278*, 1235–1252.

Berner, R. A., and G. R. Holdren (1977), Mechanism of feldspar weathering: Some observational evidence, *Geology*, *5*, 369–372.

Burns, R. G., and D. S. Fisher (1993), Rates of oxidative weathering on the surface of Mars, *J. Geophys. Res.*, *98*, 3365–3372, doi:10.1029/92JE02055.

Calas, G., G. S. Henderson, and J. F. Stebbins (2006), Glasses and melts: Linking geochemistry and materials science, *Elements*, *2*, 265–268, doi:10.2113/gselements.2.5.265.

Casey, W. H., H. R. Westrich, G. W. Arnold, and J. F. Banfield (1989a), The surface chemistry of dissolving labradorite feldspar, *Geochim. Cosmochim. Acta*, *53*(4), 821–832, doi:10.1016/0016-7037(89)90028-8.

Casey, W. H., H. R. Westrich, T. Massis, J. F. Banfield, and G. W. Arnold (1989b), The surface of labradorite feldspar after acid hydrolysis, *Chem. Geol.*, *78*(3–4), 205–218, doi:10.1016/0009-2541(89)90058-2.

Casey, W. H., H. R. Westrich, J. F. Banfield, G. Ferruzzi, and G. W. Arnold (1993), Leaching and reconstruction at the surfaces of dissolving chain-silicate minerals, *Nature*, *366*(6452), 253–256, doi:10.1038/366253a0.

Chemtob, S. M., and G. R. Rossman (2014), Timescales and mechanisms of formation of amorphous silica coatings on fresh basalts at Kīlauea Volcano, Hawai'i, *J. Volcanol. Geotherm. Res.*, *286*, 41–54, doi:10.1016/j.jvolgeores.2014.08.029.

Chemtob, S. M., B. L. Jolliff, G. R. Rossman, J. M. Eiler, and R. E. Arvidson (2010), Silica coatings in the Ka'u Desert, Hawaii, a Mars analog terrain: A micromorphological, spectral, chemical, and isotopic study, *J. Geophys. Res.*, *115*, E04001, doi:10.1029/2009JE003473.

Christensen, P. R., and S. Harrison Thliveris (1993), Thermal infrared emission spectroscopy of natural surfaces: Application to desert varnish coatings on rocks, *J. Geophys. Res.*, *98*, 19,819–19,834, doi:10.1029/93JB00135.

Christensen, P. R., et al. (2001), Mars Global Surveyor Thermal Emission Spectrometer experiment: Investigation description and surface science results, *J. Geophys. Res.*, *106*, 23,823–23,871, doi:10.1029/2000JE001370.

Clark, B. C., S. L. Kenley, D. L. O'Brien, G. R. Huss, R. Mack, and A. K. Baird (1979), Heterogeneous phase reactions of Martian volatiles with putative regolith minerals, *J. Molecular Evol.*, *14*(1–3), 91–102.

Clark, R. N., T. V. V. King, M. Klejwa, G. A. Swayze, and N. Vergo (1990), High spectral resolution reflectance spectroscopy of minerals, *J. Geophys. Res.*, *95*, 12,653–12,680, doi:10.1029/JB095iB08p12653.

Cloutis, E. A., et al. (2015), The Canadian space agency planetary analogue materials suite, *Planet. Space Sci.*, *119*, 155–172, doi:10.1016/j.pss.2015.09.001.

Crisp, J. A., A. B. Kahle, and E. A. Abbott (1990), Thermal infrared spectral character of Hawaiian basaltic glasses, *J. Geophys. Res.*, *95*, 21,657–21,669, doi:10.1029/JB095iB13p21657.

Crovisier, J. L., J. Honnorez, and J. P. Eberhart (1987), Dissolution of basaltic glass in seawater: Mechanism and rate, *Geochim. Cosmochim. Acta*, *51*(11), 2977–2990, doi:10.1016/0016-7037(87)90371-1.

Daval, D., et al. (2011), Influence of amorphous silica layer formation on the dissolution rate of olivine at 90°C and elevated pCO_2, *Chem. Geol.*, *284*(1–2), 193–209, doi:10.1016/j.chemgeo.2011.02.021.

Dixon, J. C., C. E. Thorn, R. G. Darmody, and S. W. Campbell (2002), Weathering rinds and rock coatings from an Arctic alpine environment, northern Scandinavia, *Bull. Geol. Soc. Am.*, *114*(2), 226–238, doi:10.1130/0016-7606(2002)114<0226:WRARCF>2.0.CO;2.

Doremus, R. H. (1975), Interdiffusion of hydrogen and alkali ions in a glass surface, *J. Non Cryst. Solids*, *19*(C), 137–144, doi:10.1016/0022-3093(75)90079-4.

Dorn, R. (1998), Rock Coatings, Elsevier, Amsterdam.

Farnan, I., S. C. Kohn, and R. Dupree (1987), A study of the structural role of water in hydrous silica glass using cross-polarisation magic angle spinning NMR, *Geochim. Cosmochim. Acta*, *51*(10), 2869–2873, doi:10.1016/0016-7037(87)90165-7.

Farr, T. G., and J. B. Adams (1984), Rock coatings in Hawaii, *Geol. Soc. Am. Bull.*, *95*(9), 1077–1083, doi:10.1130/0016-7606(1984)95<1077:RCIH>2.0.CO;2.

Fisk, R., M. J.-L. Crovisier, and J. Honnorez (2013), Experimental abiotic alteration of igneous and manufactured glasses, *C. R. Geosci.*, *345*(4), 176–184.

Ganguly, J., R. N. Bhattacharya, and S. Chakraborty (1988), Convolution effect in the determination of compositional profiles and diffusion-coefficients by microprobe step scans, *Am. Mineral.*, *73*(7–8), 901–909.

Geisler, T., A. Janssen, D. Scheiter, T. Stephan, J. Berndt, and A. Putnis (2010), Aqueous corrosion of borosilicate glass under acidic conditions: A new corrosion mechanism, *J. Non Cryst. Solids*, *356*(28–30), 1458–1465, doi:10.1016/j.jnoncrysol.2010.04.033.

Geisler, T., T. Nagel, M. R. Kilburn, A. Janssen, J. P. Icenhower, R. O. C. Fonseca, M. Grange, and A. A. Nemchin (2015), The mechanism of borosilicate glass corrosion revisited, *Geochim. Cosmochim. Acta*, *158*, 112–129, doi:10.1016/j.gca.2015.02.039.

Gin, S., J. V. Ryan, D. K. Schreiber, J. Neeway, and M. Cabié (2013), Contribution of atom-probe tomography to a better understanding of glass alteration mechanisms: Application to a nuclear glass specimen altered 25 years in a granitic environment, *Chem. Geol.*, *349–350*, 99–109, doi:10.1016/j.chemgeo.2013.04.001.

Gislason, S. R., and E. H. Oelkers (2003), Mechanism, rates, and consequences of basaltic glass dissolution: II. An experimental study of the dissolution rates of basaltic glass as a function of pH and temperature, *Geochim. Cosmochim. Acta*, *67*(20), 3817–3832, doi:10.1016/S0016-7037(00)00176-5.

Golden, D. C., D. W. Ming, R. V. Morris, and S. A. Mertzman (2005), Laboratory-simulated acid-sulfate weathering of basaltic materials: Implications for formation of sulfates at Meridiani Planum and Gusev crater, Mars, *J. Geophys. Res.*, *110*, E12S07, doi:10.1029/2005JE002451.

Guy, C., and J. Schott (1989), Multisite surface reaction versus transport control during the hydrolysis of a complex oxide, *Chem. Geol.*, *78*(3–4), 181–204, doi:10.1016/0009-2541(89)90057-0.

Hausrath, E. M., A. K. Navarre-Sitchler, P. B. Sak, C. I. Steefel, and S. L. Brantley (2008), Basalt weathering rates on Earth and the duration of liquid water on the plains of Gusev Crater, Mars, *Geology*, *36*(1), 67–70, doi:10.1130/G24238A.1.

Hellmann, R., J. M. Penisson, R. L. Hervig, J. H. Thomassin, and M. F. Abrioux (2003), An EFTEM/HRTEM high-resolution study of the near surface of labradorite feldspar altered at acid pH: Evidence for interfacial dissolution-reprecipitation, *Phys. Chem. Mineral.*, *30*(4), 192–197, doi:10.1007/s00269-003-0308-4.

Hellmann, R., J.-M. Penisson, R. L. Hervig, J.-H. Thomassin, and M. F. Abrioux (2004), Chemical alteration of feldspar: A comparative study using SIMS and HRTEM/EFTEM, in *Water Rock Interaction*, edited by R. B. Wanty and R. R. Seal II, pp. 753–756, Taylor and Francis Group, London.

Hellmann, R., R. Wirth, D. Daval, J. P. Barnes, J. M. Penisson, D. Tisserand, T. Epicier, B. Florin, and R. L. Hervig (2012), Unifying natural and laboratory chemical weathering with interfacial dissolution-reprecipitation: A study based on the nanometer-scale chemistry of fluid-silicate interfaces, *Chem. Geol.*, *294–295*, 203–216, doi:10.1016/j.chemgeo.2011.12.002.

Henderson, G. S. (2005), The structure of silicate melts: A glass perspective, *Can. Mineral.*, *43*(6), 1921–1958, doi:10.2113/gscanmin.43.6.1921.

Horgan, B., and J. F. Bell (2012), Widespread weathered glass on the surface of Mars, *Geology*, *40*(5), 391–394, doi:10.1130/G32755.1.

Horgan, B. H. N., R. J. Smith, E. A. Cloutis, P. Mann, and P. R. Christensen (2017), Acidic weathering of basalt and basaltic glass: 1. Near-infrared spectra, thermal infrared spectra, and implications for Mars, *J. Geophys. Res. Planets*, *122*, doi:10.1002/2016JE005111.

Hurowitz, J. A., and S. M. McLennan (2007), A ~3.5 Ga record of water-limited, acidic weathering conditions on Mars, *Earth and Planet. Sci. Lett.*, *260*(3–4), 432–443.

Hurowitz, J. A., W. W. Fischer, N. J. Tosca, and R. E. Milliken (2010), Origin of acidic surface waters and the evolution of atmospheric chemistry on early Mars, *Nat. Geosci.*, *3*(5), 323–326.

Jonas, L., T. John, H. E. King, T. Geisler, and A. Putnis (2014), The role of grain boundaries and transient porosity in rocks as fluid pathways for reaction front propagation, *Earth Planet. Sci. Lett.*, *386*, 64–74, doi:10.1016/j.epsl.2013.10.050.

Kahle, A. B., A. R. Gillespie, E. A. Abbott, M. J. Abrams, R. E. Walker, G. Hoover, and J. P. Lockwood (1988), Relative dating of Hawaiian lava flows using multispectral thermal infrared images: A new tool for geologic mapping of young volcanic terranes, *J. Geophys. Res.*, *93*, 15,239–15,251, doi:10.1029/JB093iB12p15239.

King, H. E., O. Plümper, T. Geisler, and A. Putnis (2011), Experimental investigations into the silicification of olivine: Implications for the reaction mechanism and acid neutralization, *Am. Mineral.*, *96*(10), 1503–1511, doi:10.2138/am.2011.3779.

Kraft, M. D., J. R. Michalski, and T. G. Sharp (2003), Effects of pure silica coatings on thermal emission spectra of basaltic rocks: Considerations for Martian surface mineralogy, *Geophys. Res. Lett.*, *30*(24), 2288, doi:10.1029/2003GL018848.

Kraft, M. D., T. G. Sharp, J. R. Michalski, and E. B. Rampe (2007), A pedogenic weathering model for the formation of silica coatings on high-latitude Martian surfaces, Seventh Int. Conf. on Mars, Abstract 3396.

Langer, K. and O. W. FlÖrke (1974), Near infrared absorption spectra (4000-9000cm-1) of opals and the role of "water" in these $SiO_2 \cdot nH_2O$ minerals, *Fortschr. Mineral.*, *52*(1), 17–51.

Luce, R. W., R. W. Bartlett, and G. A. Parks (1972), Dissolution kinetics of magnesium silicates, *Geochim. Cosmochim. Acta*, *36*, 35–50.

Michalski, J. R., S. J. Reynolds, T. G. Sharp, and P. R. Christensen (2004), Thermal infrared analysis of weathered granitic rock compositions in the Sacaton Mountains, Arizona: Implications for petrologic classifications from thermal infrared remote-sensing data, *J. Geophys. Res.*, *109*, E03007, doi:10.1029/2003JE002197.

Michalski, J., M. Kraft, T. Sharp, and P. Christensen (2006), Effects of chemical weathering on infrared spectra of Columbia River Basalt and spectral interpretations of Martian alteration, *Earth Planet. Sci. Lett.*, *248*(3–4), 822–829, doi:10.1016/j.epsl.2006.06.034.

Michalski, J. R., M. D. Kraft, T. G. Sharp, L. B. Williams, and P. R. Christensen (2005), Mineralogical constraints on the high-silica Martian surface component observed by TES, *Icarus*, *174*(1), 161–177, doi:10.1016/j.icarus.2004.10.022.

Milliken, R. E., et al. (2008), Opaline silica in young deposits on Mars, *Geology*, *36*(11), 847–850, doi:10.1130/G24967A.1.

Minitti, M. E., C. M. Weitz, M. D. Lane, and J. L. Bishop (2007), Morphology, chemistry, and spectral properties of Hawaiian rock coatings and implications for Mars, *J. Geophys. Res.*, *112*, E05015, doi:10.1029/2006JE002839.

Nesbitt, H. W., and I. J. Muir (1988), SIMS depth profiles of weathered plagioclase and processes affecting dissolved Al and Si in some acidic soil solutions, *Nature*, *334*, 336–338.

Niles, P. B., and J. Michalski (2009), Meridiani Planum sediments on Mars formed through weathering in massive ice deposits, *Nat. Geosci.*, *2*(3), 215–220.

Oelkers, E. H. (2001), General kinetic description of multioxide silicate mineral and glass dissolution, *Geochim. Cosmochim. Acta*, *65*(21), 3703–3719, doi:10.1016/S0016-7037(01)00710-4.

Oelkers, E. H., and S. R. Gislason (2001), The mechanism, rates, and consequences of basaltic glass dissolution: I. An experimental study of the dissolution rates of basaltic glass as a function of aqueous Al, Si and oxalic acid concentration at 25°C and pH = 3 and 11, *Geochim. Cosmochim. Acta*, *65*(21), 3671–3681, doi:10.1016/S0016-7037(00)00176-5.

O'Neil, J., and H. Taylor (1967), The oxygen isotope and cation exchange chemistry of feldspars, *Am. Mineral.*, *52*(1431), 1414–1437.

Paces, T. (1973), Steady-state kinetics and equilibrium between ground water and granitic rock, *Geochim. Cosmochim. Acta*, *37*(12), 2641–2663, doi:10.1016/0016-7037(73)90270-6.

Petit, J. C., J. C. Dran, A. Paccagnella, and G. Della Mea (1989), Structural dependence of crystalline silicate hydration during aqueous dissolution, *Earth Planet. Sci. Lett.*, *93*(2), 292–298, doi:10.1016/0012-821X(89)90077-0.

Petit, J. C., G. Della Mea, J. C. Dran, M. C. Magonthier, P. A. Mando, and A. Paccagnella (1990), Hydrated-layer formation during dissolution of complex silicate glasses and minerals, *Geochim. Cosmochim. Acta*, *54*(7), 1941–1955, doi:10.1016/0016-7037(90)90263-K.

Pollok, K., C. V. Putnis, and A. Putnis (2011), Mineral replacement reactions in solid solution-aqueous solution systems: Volume changes, reactions paths and end-points using the example of model salt systems, *Am. J. Sci.*, *311*(3), 211–236, doi:10.2475/03.2011.02.

Putnis, A., and C. V. Putnis (2007), The mechanism of reequilibration of solids in the presence of a fluid phase, *J. Solid State Chem.*, *180*(5), 1783–1786, doi:10.1016/j.jssc.2007.03.023.

Putnis, C. V., and E. Ruiz-Agudo (2013), The mineral-water interface: Where minerals react with the environment, *Elements*, *9*(3), 177–182, doi:10.2113/gselements.9.3.177.

Rice, M. S., E. A. Cloutis, J. F. Bell, D. L. Bish, B. H. Horgan, S. A. Mertzman, M. A. Craig, R. W. Renaut, B. Gautason, and B. Mountain (2013), Reflectance spectra diversity of silica-rich materials: Sensitivity to environment and implications for detections on Mars, *Icarus*, *223*(1), 499–533, doi:10.1016/j.icarus.2012.09.021.

Rogers, A. D., and P. R. Christensen (2007), Surface mineralogy of Martian low-albedo regions from MGS-TES data: Implications for upper crustal evolution and surface alteration, *J. Geophys. Res.*, *112*, E01003, doi:10.1029/2006JE002727.

Ruff, S. W., P. R. Christensen, P. W. Barbera, and D. L. Anderson (1997), Quantitative thermal emission spectroscopy of minerals: A laboratory technique for measurement and calibration, *J. Geophys. Res.*, *102*, 14,899–14,913, doi:10.1029/97JB00593.

Ruff, S. W., et al. (2011), Characteristics, distribution, origin, and significance of opaline silica observed by the Spirit rover in Gusev crater, Mars, *J. Geophys. Res.*, *116*, E00F23, doi:10.1029/2010JE003767.

Ruiz-Agudo, E., C. V. Putnis, and A. Putnis (2014), Coupled dissolution and precipitation at mineral-fluid interfaces, *Chem. Geol.*, *383*, 132–146, doi:10.1016/j.chemgeo.2014.06.007.

Ruiz-Agudo, E., C. V. Putnis, C. Rodriguez-Navarro, and A. Putnis (2012), Mechanism of leached layer formation during chemical weathering of silicate minerals, *Geology*, *40*(10), 947–950, doi:10.1130/G33339.1.

Schott, J., R. A. Berner, and E. L. Sjöberg (1981), Mechanism of pyroxene and amphibole weathering—I. Experimental studies of iron-free minerals, *Geochim. Cosmochim. Acta*, *45*(11), 2123–2135, doi:10.1016/0016-7037(81)90065-X.

Schott, J., O. S. Pokrovsky, and E. H. Oelkers (2009), The link between mineral dissolution/precipitation kinetics and solution chemistry, *Rev. Mineral. Geochem.*, *70*(1), 207–258, doi:10.2138/rmg.2009.70.6.

Schott, J., O. S. Pokrovsky, O. Spalla, F. Devreux, A. Gloter, and J. A. Mielczarski (2012), Formation, growth and transformation of leached layers during silicate minerals dissolution: The example of wollastonite, *Geochim. Cosmochim. Acta*, *98*, 259–281, doi:10.1016/j.gca.2012.09.030.

Schweda, P., L. Sjöberg, and U. Södervall (1997), Near-surface composition of acid-leached labradorite investigated by SIMS, *Geochim. Cosmochim. Acta*, *61*(10), 1985–1994, doi:10.1016/S0016-7037(97)00074-4.

Seelos, K. D., R. E. Arvidson, B. L. Jolliff, S. M. Chemtob, R. V. Morris, D. W. Ming, and G. A. Swayze (2010), Silica in a Mars analog environment: Ka'u Desert, Kilauea Volcano, Hawaii, *J. Geophys. Res.*, *115*, E00D15, doi:10.1029/2009JE003347.

Settle, M. (1979), Formation and deposition of volcanic sulfate aerosols on Mars, *J. Geophys. Res.*, *84*, 8343–8354, doi:10.1029/JB084iB14p08343.

Shotyk, W., and H. W. Nesbitt (1992), Incongruent and congruent dissolution of plagioclase feldspar: Effect of feldspar composition and ligand complexation, *Geoderma*, *55*(1–2), 55–78, doi:10.1016/0016-7061(92)90005-R.

Tanaka, K. L., J. A. P. Rodriguez, J. A. Skinner, M. C. Bourke, C. M. Fortezzo, K. E. Herkenhoff, E. J. Kolb, and C. H. Okubo (2008), North polar region of Mars: Advances in stratigraphy, structure, and erosional modification, *Icarus*, *196*(2), 318–358, doi:10.1016/j.icarus.2008.01.021.

Tosca, N. J., S. M. McLennan, D. H. Lindsley, and M. A. A. Schoonen (2004), Acid-sulfate weathering of synthetic Martian basalt: The acid fog model revisited, *J. Geophys. Res.*, *109*, E05003, doi:10.1029/2003JE002218.

Tosca, N. J., S. M. McLennan, B. C. Clark, J. P. Grotzinger, J. A. Hurowitz, A. H. Knoll, C. Schröder, and S. W. Squyres (2005), Geochemical modeling of evaporation processes on Mars: Insight from the sedimentary record at Meridiani Planum, *Earth Planet. Sci. Lett.*, *240*(1), 122–148, doi:10.1016/j.epsl.2005.09.042.

Tsomaia, N., S. L. Brantley, J. P. Hamilton, C. G. Pantano, and K. T. Mueller (2003), NMR evidence for formation of octahedral and tetrahedral Al and repolymerization of the Si network during dissolution of aluminosilicate glass and crystal, *Am. Mineral.*, *88*(1), 54–67.

White, W. B., and D. G. Minser (1984), Raman spectra and structure of natural glasses, *J. Non Cryst. Solids*, *67*(1–3), 45–59, doi:10.1016/0022-3093(84)90140-6.

Yant, M., A. D. Rogers, H. Nekvasil, Y.-Y. S. Zhao, and T. Bristow (2016), Spectral characterization of acid weathering products on Martian basaltic glass, *J. Geophys. Res. Planets*, *121*, 516–541, doi:10.1002/2015JE004969.

Zent, A. P., and C. P. McKay (1994), The chemical reactivity of the Martian soil and implications for future missions, *Icarus*, *108*, 146–157, doi:10.1006/icar.1994.1047.